JOURNAL OF GEOPHYSICAL RESEARCH, VOL. 102, NO. C8, PAGES 18,607–18,625, AUGUST 15, 1997

Inherent optical property inversion of ocean color spectra and its biogeochemical interpretation 1. Time series from the Sargasso Sea

Sara A. Garver and David A. Siegel

Institute for Computational Earth System Science and Department of Geography, University of California, Santa Barbara

Abstract. A nonlinear statistical method for the inversion of ocean color spectra is used to determine three inherent optical properties (IOPs), the absorption coefficients for phytoplankton and dissolved and detrital materials, and the backscattering coefficient due to particulates. The inherent optical property inversion model assumes that (1) the relationship between remote-sensing reflectance and backscattering and absorption is well known, (2) the optical coefficients for pure water are known, and (3) the spectral shapes of the specific absorption coefficients for phytoplankton and dissolved and detrital materials and the specific backscattering coefficient for particulates are known. This leaves the magnitudes for the three unknown coefficients to be determined. A sensitivity analysis is conducted to determine the best IOP model configuration for the Sargasso Sea using existing bio-optical models. The optical and biogeochemical measurements used were collected as part of the Bermuda Bio-Optics Project and the U.S. Joint Global Ocean Flux Study Bermuda Atlantic Time Series (BATS). The results demonstrate that the IOP model is most sensitive to changes in the exponential decay constant used to model absorption by dissolved and detrital materials. The retrieved chlorophyll *a* estimates show excellent correspondence to chlorophyll *a* determinations ($r^2 = 81\%$), similar to estimates from standard band ratio pigment algorithms, while providing two additional retrievals simultaneously. The temporal signal of retrieved estimates of absorption by colored dissolved and detrital materials is mirrored in ratios of $K_d(410)$ to $K_d(488)$, a qualitative indicator for nonalgal light attenuation coefficients. The backscatter coefficient for particles is nearly constant in time and shows no correspondence with the temporal signal observed for chlorophyll *a* concentrations. Last, the IOP model is evaluated using only those wavelengths which closely match the Sea Viewing Wide Field of View Sensor wave bands. This results in only a 1 to 6% decrease in hindcast skill with the BATS biogeochemical data set. This is encouraging for the long-range goal of applying the IOP model to data from upcoming ocean color satellite missions.

1. Introduction

The images produced by the coastal zone color scanner (CZCS) provided new insights for biological oceanographers and gave unprecedented information about the marine biosphere [*Gordon and Morel*, 1983; *Mitchell*, 1994]. However, this instrument was primarily used to determine only a single index, the chlorophyll pigment concentration, to describe the entire functioning of the ocean's ecosystem. This is clearly not enough information to explain all the important biogeochemical processes in the ocean such as the cycling of carbon and nitrogen and predictions of regional fishery yields.

Ocean color observations can and should yield more information than simply the single chlorophyll pigment concentration. Here we use a nonlinear statistical method for the inversion of ocean color spectra to produce three relevant inherent optical properties (IOPs) for the analysis of biogeochemical variability: the absorption coefficient by phytoplankton, the absorption coefficient by dissolved and detrital materials, and the backscattering coefficient due to particulates. Methods to invert ocean color observations, such as those employed here, have been extensively explored by *Morel and Prieur* [1977], *Sugihara et al.* [1985], *Sathyendranath et al.* [1989], *Gordon et al.* [1988], and *Roesler and Perry* [1995].

The color of the sea will be related to those photons which are backscattered from within the water column and are not absorbed before entering the atmosphere. Hence changes in the total absorption coefficient, $a(\lambda)$ (notation list is provided), and the backscattering coefficient, $b_b(\lambda)$, regulate the variations in ocean color spectra or remotely sensed reflectance $[R_{rs}(\lambda)]$, where $R_{rs}(\lambda)$ is defined as the ratio of upwelled radiance to downwelled irradiance $(=L_u(\lambda)/E_d(\lambda))$. Values of $a(\lambda)$ an be effectively partitioned into absorption due to water, phytoplankton, and nonalgal materials [e.g., *Kishino et al., 1984*; *Carder et al.*, 1989; *Garver et al.*, 1994]. The value of $b_b(\lambda)$ is typically much smaller than $a(\lambda)$ for case I waters [*Gordon et al., 1988*]. In addition, there are no a priori reasons why absorption and scattering properties should be well correlated [*Kitchen and Zaneveld*, 1990].

Theoretical studies have shown that remote-sensing reflectance can be related to the IOPs of the water column, which in turn are composed of the individual absorbers and scatterers, including water, particulates, and dissolved materials. Hence IOPs can be used to study upper ocean

Paper number 96JC03243.
0148-0227/97/96JC-03243$09.00

biological processes, including phytoplankton distributions, primary production rates, and biogenic gas fluxes. Ocean color observations can be either remotely sensed ($R_{rs}(0^+,\lambda)$, as by the upcoming sea viewing wide field of view sensor (SeaWiFS) or ocean color thermal sensor (OCTS) missions, or obtained in situ ($R_{rs}(z,\lambda)$), such as in the Bermuda Bio-Optics Program (BBOP) [*Siegel et al.*, 1995a,b]. Remotely sensed ocean color observations have the advantage of providing basin scale coverage of the upper mixed layer, while in situ observations provide high vertical resolution (ship) and/or high temporal (mooring) coverage [e.g., *Smith et al.*, 1987; *Dickey*, 1991].

We demonstrate that an IOP inversion approach for the analysis of ocean color spectra can be successfully applied in the blue ocean and that the retrievals provide useful information for the evaluation of the functioning of the biogeochemical system in the Sargasso Sea. This region is an excellent location to investigate biogeochemical processes on monthly to interannual timescales due to the strong seasonal variations in ocean biogeochemical cycles [e.g., *Menzel and Ryther*, 1960, 1961; *Siegel et al.*, 1995a; *Michaels et al., 1994*]. To evaluate the IOP inversion model, we assess its capabilities as a chlorophyll *a* model, examine the temporal changes in nonalgal absorption, assess the modeling and potential sources of the particulate backscatter coefficient, and evaluate the application of the IOP model to upcoming satellite ocean color imagery.

2. Modeling Methodology

The goal of the IOP inversion model is to maximize the information that can be extracted from ocean color observations. For this study, the IOP inversion model is applied to in situ observations of $R_{rs}(\lambda)$ from the Bermuda Bio-Optics Project [*Siegel et al.*, 1995a,b]. The model is general enough to be applied to other oceanic regions with confidence in its success and has the advantage of providing measures of uncertainty for the modeled inherent optical properties.

The IOP inversion model is based upon the following three assumptions. First, the relationship between $R_{rs}(\lambda)$ and $b_b(\lambda)$ and $a(\lambda)$ is assumed to be well known. Second, the optical coefficients for pure water, $a_w(\lambda)$ and $b_{bw}(\lambda)$, are known [*Smith and Baker*, 1981]. Last, the spectral shapes of the specific absorption coefficients for phytoplankton and non-algal materials and the specific backscattering coefficient for particulates, $a_{ph}^*(\lambda)$, $a_{dm}^*(\lambda)$, and $b_{bp}^*(\lambda)$, are known functions of their magnitudes (please note that the asterisks are used to indicate these are spectral shapes; see notation list). Knowing these factors, the magnitudes of the unknown absorption and backscattering coefficients may be determined.

The IOP inversion model assumes that the relationship between $R_{rs}(\lambda)$ and the ratio of backscattering to absorption coefficients is known and stable, for example,

$$R_{rs}(\lambda) \equiv \frac{L_u(\lambda)}{E_d(\lambda)} \cong \sum_{i=1}^{2} l_i \left[\frac{b_b(\lambda)}{b_b(\lambda)+a(\lambda)} \right]^i \quad (1)$$

where $L_u(\lambda)$ is upwelling radiance just beneath the sea surface, $E_d(\lambda)$ is downwelling irradiance at the same depth, $l_1 = 0.0949$ sr^{-1}, and $l_2 = 0.0794$ sr^{-1} [*Gordon et al.*, 1988]. The quadratic form of (1) should be particularly important for high $R_{rs}(\lambda)$ observations such as those found in the blue Sargasso Sea. A comparison of the linear and quadratic forms of (1) demonstrates that values of $b_b(\lambda)/[a(\lambda) + b_b(\lambda)]$ from a measure of $R_{rs}(\lambda)$ could be overestimated if only the linear term in (1) is used and that difference will increase with increasing values of $R_{rs}(\lambda)$ (Figure 1). For example, a value of $R_{rs}(\lambda) = 0.01$ sr^{-1} could result in a 10% difference in the estimate of $b_b(\lambda)/[a(\lambda) + b_b(\lambda)]$, while a value of $R_{rs}(\lambda) = 0.03$ sr^{-1} might result in a 25% difference between the two model forms (Figure 1). This difference should be particularly important for clear waters with high $R_{rs}(\lambda)$ values.

The absorption and backscattering coefficients in (1) are the sums of the individual coefficients due to the absorbers and scatterers which are present and can be written as

$$b_b(\lambda) = b_{bw}(\lambda) + b_{bp}(\lambda) \quad (2)$$

where $b_{bw}(\lambda)$ is the backscatter due to pure seawater and $b_{bp}(\lambda)$ is the backscatter due to particles, and

$$a(\lambda) = a_w(\lambda) + a_{ph}(\lambda) + a_{dm}(\lambda) \quad (3)$$

where $a_w(\lambda)$ is the absorption due to seawater, $a_{ph}(\lambda)$ is the absorption due to phytoplankton, and $a_{dm}(\lambda)$ is the absorption due to the combined effects of colored dissolved and detrital materials (CDM). For our model, the spectral signatures of CDM will be modeled as a single exponential shape as the signals due to colored dissolved organic and detrital materials are likely to be inseparable [*Carder et al.*, 1991; *Siegel and Michaels*, 1996].

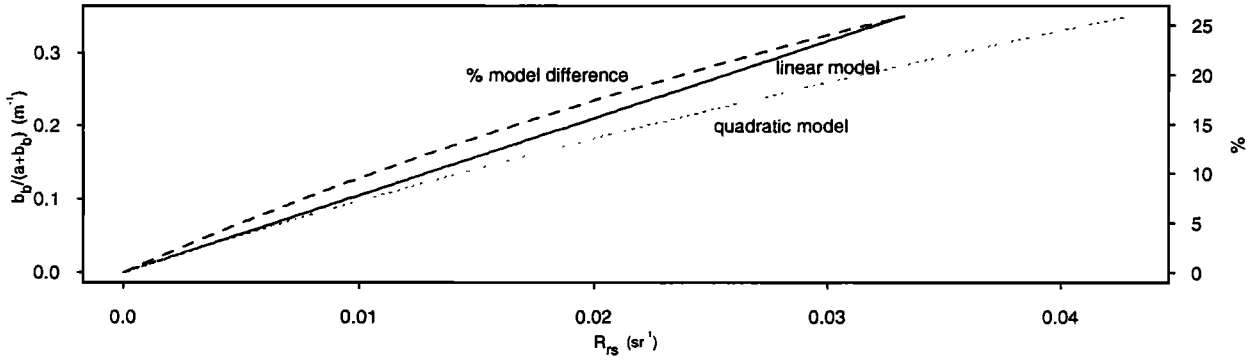

Figure 1. A comparison of the linear and quadratic forms of (1), demonstrating that values of $b_b/(a + b_b)$ from a measure of $R_{rs}(\lambda)$ will differ depending the model form used. These differences will increase with increasing values of $R_{rs}(\lambda)$; thus the quadratic form of (1) will be particularly important for high $R_{rs}(\lambda)$ observations such as those found in the blue Sargasso Sea.

The IOP inversion model assumes that values of $a_w(\lambda)$ and $b_{bw}(\lambda)$ are known (Figure 2a). The absorption and backscattering properties of pure seawater have been tabulated by *Smith and Baker* [1981]. Using values of the diffuse attenuation coefficient for irradiance in the clearest natural waters, *Smith and Baker* [1981] deduced proper values for the absorption coefficient of seawater. The coefficient for total scattering by seawater, $b_m^{sw}(\lambda)$, is taken from *Morel* [1974], who has reviewed in great detail the theory and observations pertaining to scattering by both pure water and pure seawater. Values of the backscattering coefficient for sea water are assumed to be equal to $1/2 b_m^{sw}(\lambda)$.

The IOP model is based upon the assumption that spectral shapes for $a_{ph}^*(\lambda)$, $a_{dm}^*(\lambda)$, and $b_{bp}^*(\lambda)$ are fixed or known

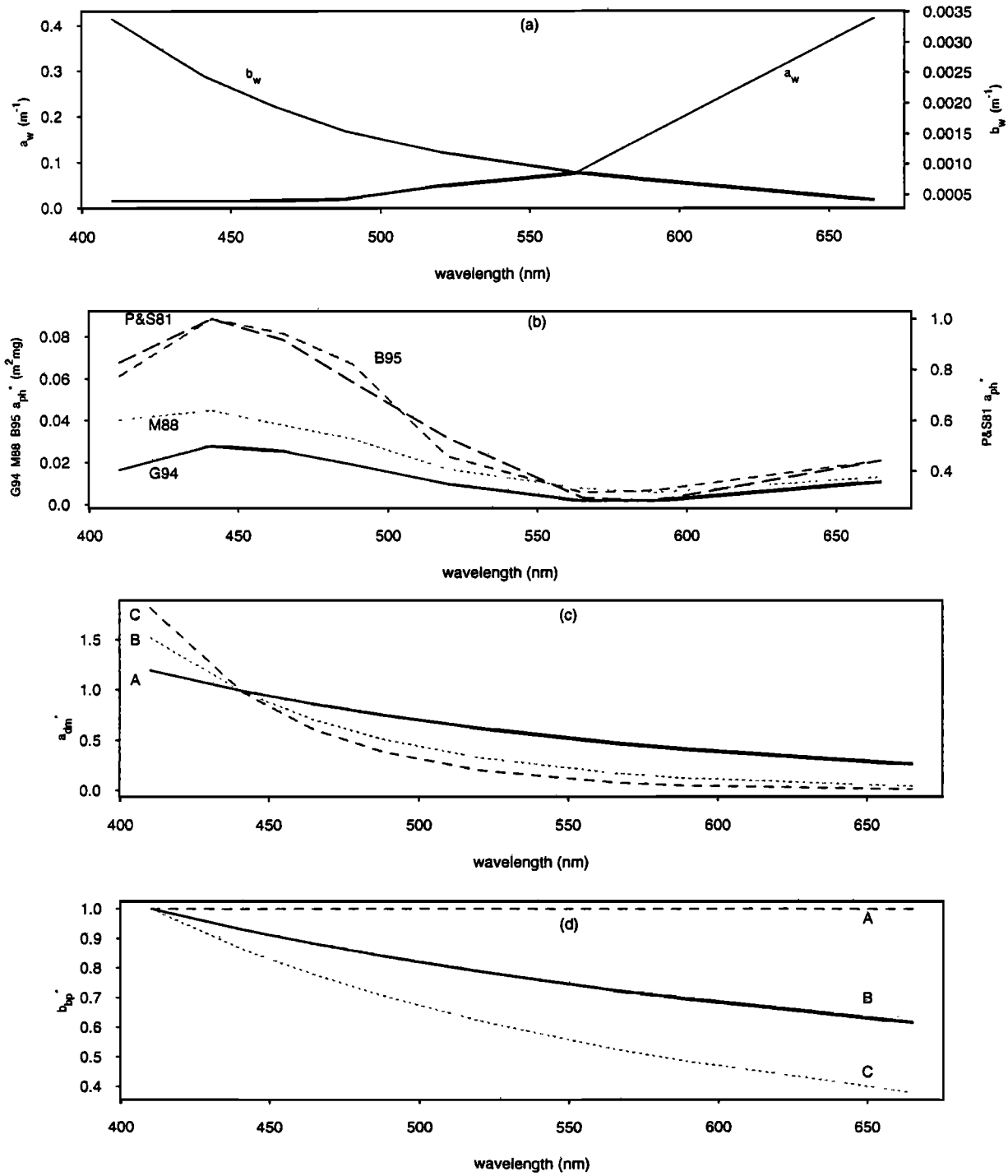

Figure 2. Known and assumed spectral shapes composing the IOP inversion model: (a) Absorption and backscattering by pure seawater ($a_w(\lambda)$ and $b_{bw}(\lambda)$). (b) Four $a_{ph}^*(\lambda)$ modeled spectra [*Prieur and Sathyendranath*, 1981; *Morel*, 1988; *Garver et al.*, 1994; *Bricaud et al.* 1995] (P&S81, M88, G94, and B95). (c) Three $a_{dm}^*(\lambda)$ modeled spectra, line A., S = -0.006, line B., S = -0.014 and line C., S= -0.020 nm^{-1}. (d) Three $b_{bp}^*(\lambda)$ modeled spectra, line A., λ^0, line B., λ^{-1}, and line C, λ^{-2}.

functions of a single index. The spectral shape of phytoplankton absorption results from the combination of the light-absorbing properties of chlorophyll *a* and other accessory pigments which absorb in specific regions of the visible spectrum (centered at 440 and 675 nm) modified by their packaging within the cell [*Kirk, 1994*]. Four $a_{ph}^*(\lambda)$ models are explored here [*Prieur and Sathyendranath*, 1981; *Morel*, 1988; *Garver et al.*, 1994; *Bricaud et al.*, 1995] (Figure 2b). The *Prieur and Sathyendranath* [1981] $a_{ph}^*(\lambda)$ model was statistically derived from 90 spectral absorption coefficients which were calculated using upwelling and downwelling irradiance values from various case I marine regions. The *Morel* [1988] $a_{ph}^*(\lambda)$ model was obtained by averaging values of 14 cultured phytoplankton species. The *Garver et al.* [1994] $a_{ph}^*(\lambda)$ model was obtained from the partitioning of an extensive database of particulate absorption spectra assembled from 11 cruises in the Atlantic and Pacific, both open ocean and coastal, using the multidimensional regression model of *Morrow et al.* [1989]. The *Bricaud et al.* [1995] $a_{ph}^*(\lambda)$ model was developed as a power law fit with respect to chlorophyll *a* of 815 $a_{ph}(\lambda)$ spectra measured using the filter pad and methanol extraction techniques. The shapes of the modeled $a_{ph}^*(\lambda)$ spectra are all constant except for the *Bricaud et al.* [1995] model which is a function of the chlorophyll *a* concentration.

In contrast, the CDM component of absorption is modeled as an exponential function which decreases with increasing wavelength [*Carder et al.*, 1991; *Roesler et al.*, 1989], or

$$a_{dm}(\lambda) = a_{dm}(\lambda_0)\exp[S(\lambda-\lambda_0)] \tag{4}$$

where $a_{dm}(\lambda_0)$ is the absorption by CDM at a reference wavelength, $\lambda_0 = 440$ nm, and values of S, the exponential decay constant, were chosen to span values found in the literature (S = -0.006, -0.014, and -0.020 nm^{-1}; Figure 2c).

Backscattering in the oceans by marine particulates has only recently been studied in detail, and it is clear that there is a spectral signature and that scattering and backscattering in particular vary greatly for different types of particulates. It appears that marine particles of the order of 1 μm in diameter and smaller are the major source of backscattering in the open ocean. Living organisms in this size range include viruses, heterotrophic and photoautotrophic bacteria, and small eucaryotic algal cells, as well as inanimate detrital particles [*Stramski and Kiefer*, 1991; *Morel and Ahn*, 1991]. Direct measurements of $b_b(\lambda)$ for phytoplankton cultures support the notion of insignificantly low values of algal backscatter coefficients for case I waters [*Bricaud et al.*, 1983; *Ahn et al.*, 1992]. An exception to this is the nanoplankton-sized coccolithophores and in particular detached coccoliths, which have a characteristically large backscatter signal [*Balch et al.*, 1991].

Experimental data and theory indicate that under most conditions, values of $b_{bp}(\lambda)$ decrease monotonically with respect to wavelength. Three power law spectra, going as λ^0,λ^{-1}, and λ^{-2} are each used individually as the $b_{bp}^*(\lambda)$ modeled spectrum (Figure 2d). The spectral signature of particulate backscatter has been commonly modeled as λ^{-1} [*Gordon and Morel*, 1983; *Morel*, 1987, 1988; *Roesler and Perry*, 1995]. However, recent work has shown that 0.2-0.5 μm size particles make the dominant contribution to particulate backscattering and should be modeled as λ^{-2} [*Stramski and Kiefer*, 1991]. The backscatter due to phytoplankton cells is both typically smaller and spectrally uniform and is modeled as λ^0 [*Bricaud et al.*, 1983; *Morel and Ahn*, 1991].

The IOP inversion model can now be rewritten (see (1)) as the summation of the various components comprising absorption and scattering:

$$\hat{R}_{rs}(\lambda) = \sum_{i=1}^{2} l_i \left[\frac{b_b(\lambda)}{b_b(\lambda)+a_w(\lambda)+Chl\,a_{ph}^*(\lambda)+a_{dm}(\lambda)exp(S(\lambda-\lambda_0))}\right]^i \tag{5}$$

where $b_b(\lambda) = b_w(\lambda) + b_{bp}(\lambda_0)b_{bp}^*(\lambda)$, $b_{bp}^*(\lambda)$ is modeled as $(\lambda/\lambda_0)^{-n}$ (n = 0, 1, 2), *Chl* is chlorophyll *a* (milligrams per cubic meter) for the *Bricaud et al.* [1995], *Morel* [1988] and *Garver et al.* [1994] $a_{ph}^*(\lambda)$ models, and *Chl* is $a_{ph}(441)$ for the *Prieur and Sathyendranath* [1981] $a_{ph}^*(\lambda)$ model. The model is inverted by overconstraining in wavelength and solving for the three unknown parameters, $b_{bp}(\lambda_0)$, *Chl*, and $a_{dm}(\lambda_0)$ By multiplying the retrieved magnitudes by the assumed shapes, IOP estimates at each wavelength can be determined.

The difficulty with the inversion procedure is that the final IOP model is nonlinear (equation (5)). A general nonlinear least squares model can be written as [*Bates and Watts, 1988*]

$$Y_n = f(x_n, \theta_p) + Z_n \tag{6}$$

where Y_n are the measured responses ($=R_{rs}(\lambda_n)$), $f(x_n, \theta_p)$ is the expectation function ($=\hat{R}_{rs}(\lambda_n)$,(5)), n is the index of realization per observation (a total of 8 wavelengths), x_n is the matrix of independent variables ($b_{bp}^*(\lambda_n)$, $a_{ph}^*(\lambda_n)$ and $a_{dm}^*(\lambda_n)$, θ_p is the array of unknown parameters ($b_{bp}(\lambda_0)$, *Chl*, and $a_{dm}(\lambda_0)$; $p = 3$), and Z_n are the model residuals. This model is of the same form as the general linear regression model, where Z_n is assumed to have a normal distribution, with the exception that the expected responses are nonlinear functions of the parameters. It is the squared sum of the residuals which is minimized by selecting the optimal array, θ_p. When analyzing a particular set of data, the matrix x_n, is fixed, and it is the dependence of the expected responses, Y_n, on the parameters, θ_p, that is of interest. For our application, a Gauss-Newton algorithm is employed which uses a linear approximation to the expectation function to iteratively improve an initial parameter guess. This iterative process continues until convergence is obtained, meaning that there is no useful change in the elements of the parameter vector [*Bates and Watts*, 1988]. The parameter estimates from the IOP model, $b_{bp}(\lambda_0)$, *Chl*, and $a_{dm}(\lambda_0)$, are then multiplied by the value of their shape spectra at 441 nm to obtain estimates of the three IOPs, $a_{ph}(441)$, $a_{dm}(441)$, and $b_{bp}(441)$. For example, $a_{ph}(441) = Chl\,a_{ph}^*(441)$. Standard errors for the parameter estimates are determined by evaluating the derivative matrix at the least squares parameter estimates. Using the standard errors associated with these estimates, an interval of values that is likely to contain the true value of the IOPs can then be obtained. These 1-α confidence intervals are calculated for each of the modeled IOPs at the 0.95 level:

$$\hat{\theta}_p \pm \sigma_e(\hat{\theta}_p)\, t(n-p;\alpha/2) \tag{7}$$

where $\sigma_e(\hat{\theta}_p)$ are the standard errors from the nonlinear regression and $t(n\text{-}p;\alpha/2)$ is the upper quantile for the Student's t distribution with n-p degrees of freedom [Bates and Watts, 1988].

To validate the IOP model, a sensitivity analysis is performed which examines the effects of varying the different modeled components composing the IOP model. This involves using the different modeled spectra for particulate and dissolved substances found in the literature ($a_{ph}^*(\lambda)$, $a_{dm}^*(\lambda)$, $b_{bp}^*(\lambda)$) in a series of model runs. The retrieved IOPs from each of these model runs are then used in linear regressions with the BATS biogeochemical data set for empirical comparison and temporal scale interpretation.

3. Data Sources

In situ optical and biogeochemical measurements from the U.S. Joint Global Ocean Flux Study (JGOFS) Bermuda Atlantic Time Series (BATS) are used in this study. Methods for these data have been presented in detail several times [*Knap et al.*, 1993; *Michaels et al.*, 1994; *Siegel et al.*, 1995b]. The BATS site is located 75 km southeast of Bermuda 31°50' N; 64°10' W) in the Sargasso Sea. Cruises are biweekly to monthly with an average of 16 per year beginning in October 1988. Optical profiles were taken as part of the Bermuda Bio-Optics Project (BBOP), which shares both ship time and water samples with BATS. Optical profiling commenced in January 1992.

Determinations of downwelling spectral irradiance and upwelling radiance are made as part of the BBOP program using a multichannel profiling spectroradiometer (BioSpherical Instruments, Inc., MER-2040 [*Smith et al.*, 1984]). This study analyzes $R_{rs}(\lambda)$ spectra from near noontime casts for 1992 and 1993. The optics casts composing the data set are taken from 37 separate dates over the 24 month period. To maximize the size of the data set, $R_{rs}(\lambda)$ are calculated for both 0^- m and 5 m depths, resulting in a total of 72 spectra; no significant differences in IOP inversion results were found between the 0^- and 5 m $R_{rs}(\lambda)$ spectra. For the data presented, the BBOP spectroradiometer measures downwelling irradiance in eight spectral bands (410, 441, 465, 488, 520, 565, 589, and 665 nm) and upwelled radiance in nine wave bands (410, 441, 465, 488, 520, 565, 589, 665, and 683 nm). Extrapolated values of downwelling irradiance and upwelling radiance just beneath the surface, $E_d(0^-,\lambda)$ and $L_u(0^-,\lambda)$, are calculated using a robust least squares formulation. In addition, values of the diffuse attenuation coefficient $K_d(\lambda)$, are calculated using measurements of $E_d(z,\lambda)$ in a least squares regression over 10 m intervals [*Siegel et al.*, 1995b].

The BBOP package is deployed ~3 m off the stern of the R/V *Weatherbird II*, which is oriented toward the Sun to most effectively reduce ship shadowing [*Mueller and Austin*, 1992]. Direct examination has shown that the effects of ship shadows are not appreciable with this deployment procedure [*Weir et al.*, 1994]. Self-shading by the spectroradiometer has also been shown to not be a problem unless $a(\lambda) \cdot R \geq 0.01$ [*Gordon and Ding*, 1992], where R is the radius of the instrument (10 cm). Thus instrument self-shading will occur only if values of $a(\lambda)$ are ≥ 0.1 m^{-1}, which at this site is only observed for wavelengths greater than 600 nm. For the analyses presented here, this source of error may be effectively ignored (see discussion section). Optical calibrations were performed every 4 to 6 months at the University of California, Santa Barbara (UCSB) ocean optics calibration facility which participates in the SeaWiFS optical calibration laboratory round robin exercises [*Mueller et al.*, 1993, 1994]. Thus the lamp radiance plaque and integrating sphere standards used to calibrate the BBOP spectroradiometer are directly traceable to the National Institute of Standards and Technology. An intercomparison between calibration facilities shows differences in calibration constants of less than 1% for $E_d(\lambda)$ and 1 to 2% for $L_u(\lambda)$ (D. Menzies, personal communication, 1995). Immersion coefficients for the BBOP irradiance collector were recently determined [*Mueller*, 1996].

The biogeochemical observations from the BATS program that will be used as a model validation data set for this study include phytoplankton pigments measured by high pressure liquid chromatography (HPLC; milligrams per cubic meter) and fluorometry (milligrams per cubic meter), mixed layer depths (meters), nutrients (nitrate and nitrite; micromoles per kilogram), particulate organic carbon (POC; micrograms per kilogram), particulate organic nitrogen (PON; micrograms per kilogram), bacterial abundance (numbers per cubic meter), and the diffuse attenuation coefficient ($K_d(\lambda)$; m^{-1}). The ratio of $K_d(410)$ to $K_d(488)$ has been shown to be a good qualitative indicator of CDM concentration [*Siegel et al.*, 1995a; *Siegel and Michaels*, 1996]. Model retrievals of $a_{ph}(441)$ and $a_{dm}(441)$ should show some level of correspondence to the BATS pigment determinations, nutrient concentrations, mixed layer depths, and the ratio of $K_d(410)$ to $K_d(488)$, while model retrievals of $b_{bp}(441)$ should correspond to the particulate fields of POC, PON, and bacteria. All the variables in the validation data set are measured within 5 m of the surface, with the exception of the $K_d(\lambda)$ data which were taken from a depth of 20 m. When possible, $R_{rs}(\lambda)$ spectra and BATS biogeochemical data are taken from the same day. For five of the spectra used, BATS pigment data are not available for that day, and data either 1 day before or after the date of the optics cast are used.

4. Results

4.1. Temporal Variation in Optical and Biogeochemical Parameters

Seasonal variations in both optical and biogeochemical observations from the BATS site are caused primarily by short-lived springtime phytoplankton blooms and periods of deep mixing. The magnitude of these blooms appears to be correlated with the intensity of winter storms, suggesting that the ventilation of 18° water and its vertical transport of new nutrients into the euphotic zone controls primary production off Bermuda. This seasonal cycle of the 18° water ventilation is an important aspect of the temporal changes in the biological properties of the Sargasso Sea [*Menzel and Ryther*, 1960, 1961; *Michaels et al.*, 1994; *Siegel et al.*, 1990, 1995a].

The BATS pigment determinations (fluorometric chlorophyll *a*, fluorometric chlorophyll *a* plus pheopigments, and HPLC chlorophyll *a*) are all extremely similar to one another and show strong seasonal variability with elevated concentrations (>0.2 mg m^{-3}) in the winter-spring months (Table 1a; Figure 3a). This is coincident with the changes in nutrient concentrations which are above detectability in the winter-spring months when mixed layer depths are at their deepest (Table 1a; Figure 4a). An annual cycle is also observed for ratios of $K_d(410)$ to $K_d(488)$, the qualitative indicator of CDM absorption, with the highest values again observed during the winter-spring months (Figure 3b) [*Siegel et al.*, 1995a; *Siegel and Michaels*, 1996]. This ratio is positively and significantly correlated with the various pigment determinations (Table 1a); however, the timing of the

Table 1a. Pearson's Correlation Coefficient of BATS Validation Data Set

	$Fl_{chl\ a+pheo}$	$HPLC_{chl\ a}$	Nutrients	MLD	Bacteria	POC	PON	K_d(410:488)
$Fl_{chl\ a}$	0.99*	0.95*	0.60*	-0.65*	0.02	0.01	0.36	0.68*
$Fl_{chl\ a+pheo}$		0.94*	0.58*	-0.68*	0.21	0.04	0.30	0.69*
$HPLC_{chl\ a}$			0.74*	-0.67*	0.09	0.11	0.30	0.61*
Nutrients				-0.23	0.11	0.19	0.25	0.37*
MLD					0.36*	0.41*	-0.11	-0.45*
Bacteria						0.69*	0.44*	0.22
POC							0.64*	0.41*
PON								0.64*

BATS validation data set includes pigments measured by flourometry and high pressure liquid chromatography ($Fl_{chl\ a}$, $Fl_{chl\ a+pheo}$, $HPLC_{chl\ a}$; milligrams per cubic meter), nutrients (nitrate and nitrite; micromoles per kilogram), mixed layer depth (MLD; meters), bacterial abundances (numbers per cubic meter), particulate organic carbon and nitrogen (POC and PON; micromoles per kilogram), ratios of K_d(410) to K_d(488).

*These correlation coefficients are significant at a level of 0.95.

seasonal cycles differs somewhat in duration (Figure 3). Weak or nonexistent seasonal cycles are observed for the POC, PON, and bacterial abundance data (Figure 4b), with positive correlation's observed among these particulate fields (Table 1a).

The temporal pattern observed for $R_{rs}(\lambda)$ also shows a strong seasonal cycle (Plate 1). Values of $R_{rs}(\lambda)$ are highest in the late spring, summer, and fall (April-November) and lowest in the winter (December-March). Thus the Sargasso Sea will be "bluer" in summer and "greener" in the winter. The R_{rs}(410-488) values for April to November are typically in the 0.015-0.025 sr^{-1} range. Therefore using a linear $R_{rs}(\lambda)$ to IOP ratio model (equation (1)) during these time periods could lead to overestimates of roughly 15 to 20% for these wavelengths

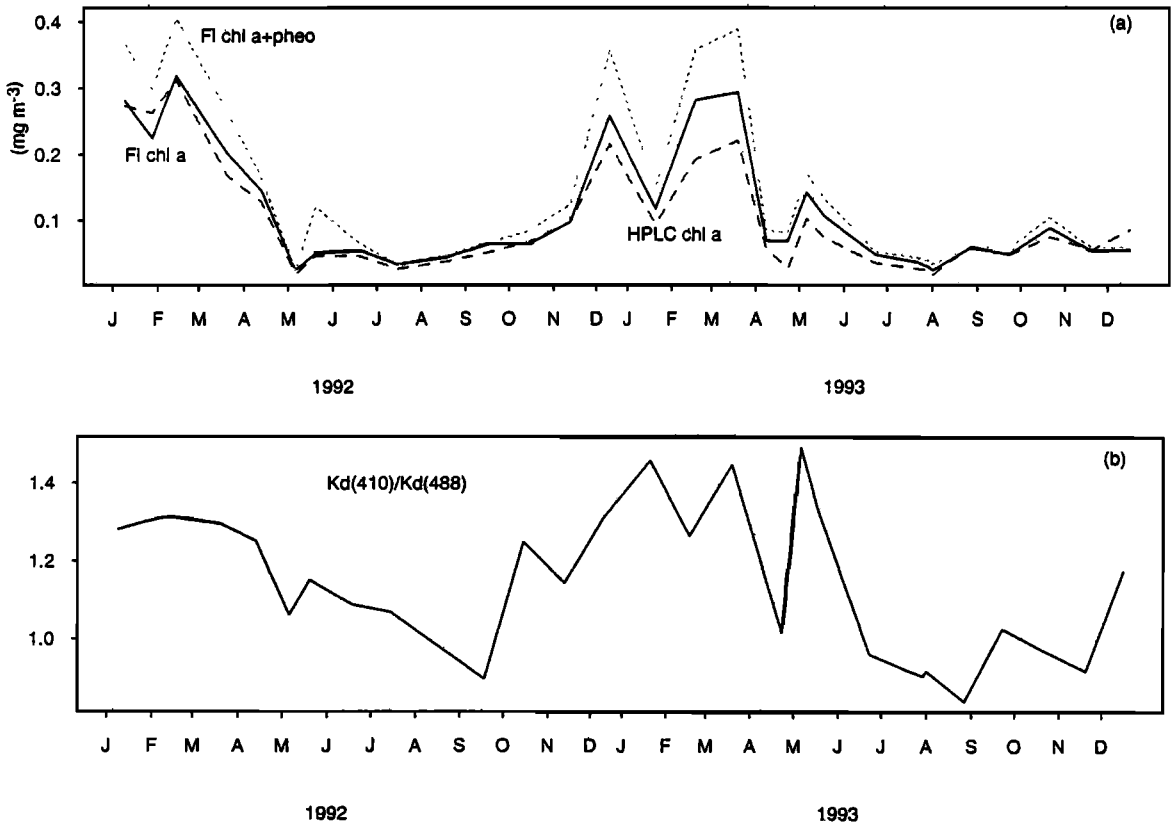

Figure 3. U.S. JGOFS Bermuda Atlantic Time Series (BATS & BBOP) data: (a) Pigment determinations (fluorometric chlorophyll *a*, fluorometric chlorophyll *a* plus pheopigments, and HPLC chlorophyll *a*; milligrams per cubic meter) and (b) Wavelength ratios of the diffuse attenuation coefficient (K_d(410) to K_d(488)).

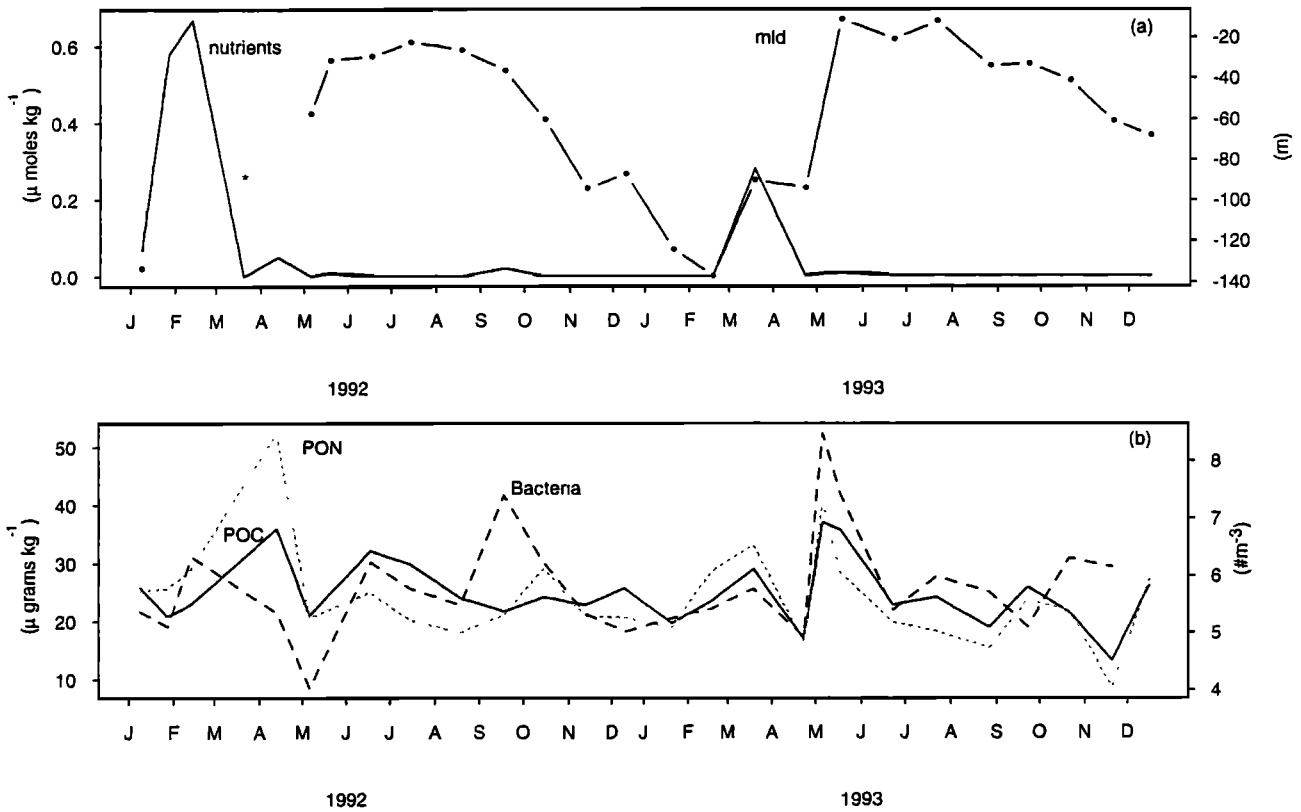

Figure 4. U.S. JGOFS Bermuda Atlantic Time Series (BATS) data: (a) Nutrient concentrations (nitrate and nitrite; micromoles per kilogram) and mixed layer depths (meters) and (b) Particulate organic carbon (POC; micrograms per kilogram), particulate organic nitrogen (PON; micrograms per kilogram), and bacterial abundance (number per cubic meter).

(Figure 1). The R_{rs}(410-488) wavelengths are the most highly correlated to the BATS variables, and demonstrate the greatest seasonal variability (Table 1b; Plate 1). Conversely, the green-red wave bands (≥520 nm) show little correlation with any of the BATS variables. The blue-green $R_{rs}(\lambda)$ distribution has strong inverse relationships with all three pigment determinations and the ratios of K_d(410) to K_d(488) (Table 1b). This relationship between $R_{rs}(\lambda)$ and both pigments and ratios of K_d(410) to K_d(488) suggests that changes in $a(\lambda)$ are primarily responsible for the temporal changes in $R_{rs}(\lambda)$. It appears that $b_b(\lambda)$ is not a significant factor in driving $R_{rs}(\lambda)$ temporally, as is demonstrated by the weak correlations between $R_{rs}(\lambda)$ observations and particulates fields such as POC and bacteria.

4.2. IOP Model Evaluation

The sensitivity analyses performed on the IOP inversion model assess the effects of varying the spectral shape components ($a_{ph}^*(\lambda)$, $a_{dm}^*(\lambda)$, $b_{bp}^*(\lambda)$) of the model. The first set of model runs begins with a base state of the particulate specific backscatter coefficient modeled as λ^{-1} and the phytoplankton specific absorption coefficient modeled using the *Morel* [1988] $a_{ph}^*(\lambda)$ spectrum. Three $a_{dm}^*(\lambda)$ spectra (S = -0.006, -0.014, -0.02 nm^{-1}) are then applied to the entire data set while holding the $a_{ph}^*(\lambda)$ and $b_{bp}^*(\lambda)$ spectra constant (Figure 5a). The S = -0.006 nm^{-1} case gives the poorest results. This is evidenced by the percent variance explained in the linear regressions between the retrieved a_{ph}(441) from this model run and the BATS pigment determinations (r^2 = 12-18%; Table 2). The other two modeled $a_{dm}^*(\lambda)$ spectra result in a significantly higher percent variance explained for the same regressions, with the S = -0.02 nm^{-1} case being slightly better than the S = -0.014 nm^{-1} case (77 to 84% versus 63 to 73%). As is shown in Figure 5a, changes in the value of the exponential decay constant, S, have a significant effect on the magnitude of the a_{ph}(441) and a_{dm}(441) retrievals and less of an effect on the b_{bp}(441) retrievals. The $a_{dm}(\lambda)$ spectrum calculated using S = -0.02 nm^{-1} is chosen to continue with the sensitivity analysis. This value of the exponential decay constant is consistent with CDM absorption spectra obtained by both *Green and Blough* [1994], who found a range of S values from -0.018 to -0.02 nm^{-1}, and *Nelson et al.* [1997] who determined an average value of S = -0.025 nm^{-1} (standard deviation = 0.004) in the Sargasso Sea.

For the second set of model runs, three $b_{bp}^*(\lambda)$ spectra (λ^0,λ^{-1},λ^{-2}) are each used in individual model runs, while holding the $a_{dm}^*(\lambda)$ and $a_{ph}^*(\lambda)$ spectra constant with S equal to -0.02 nm^{-1} and *Morel* [1988], respectively. The results of the linear regressions for this set of model runs are virtually identical (Table 3), as are the retrieved values of the three IOPs (Figure 5b). The retrieved a_{ph}(441) and a_{dm}(441) values show a strong seasonal cycle with highest values in the winter months. Retrievals of b_{bp}(441) are nonseasonal with the largest b_{bp}(441) retrievals occurring for the λ^{-1} model. The choice of the $b_{bp}^*(\lambda)$ model used has little effect on the results of the IOP inversion for this particular data set. The λ^{-1} spectra, a common representation from the literature for

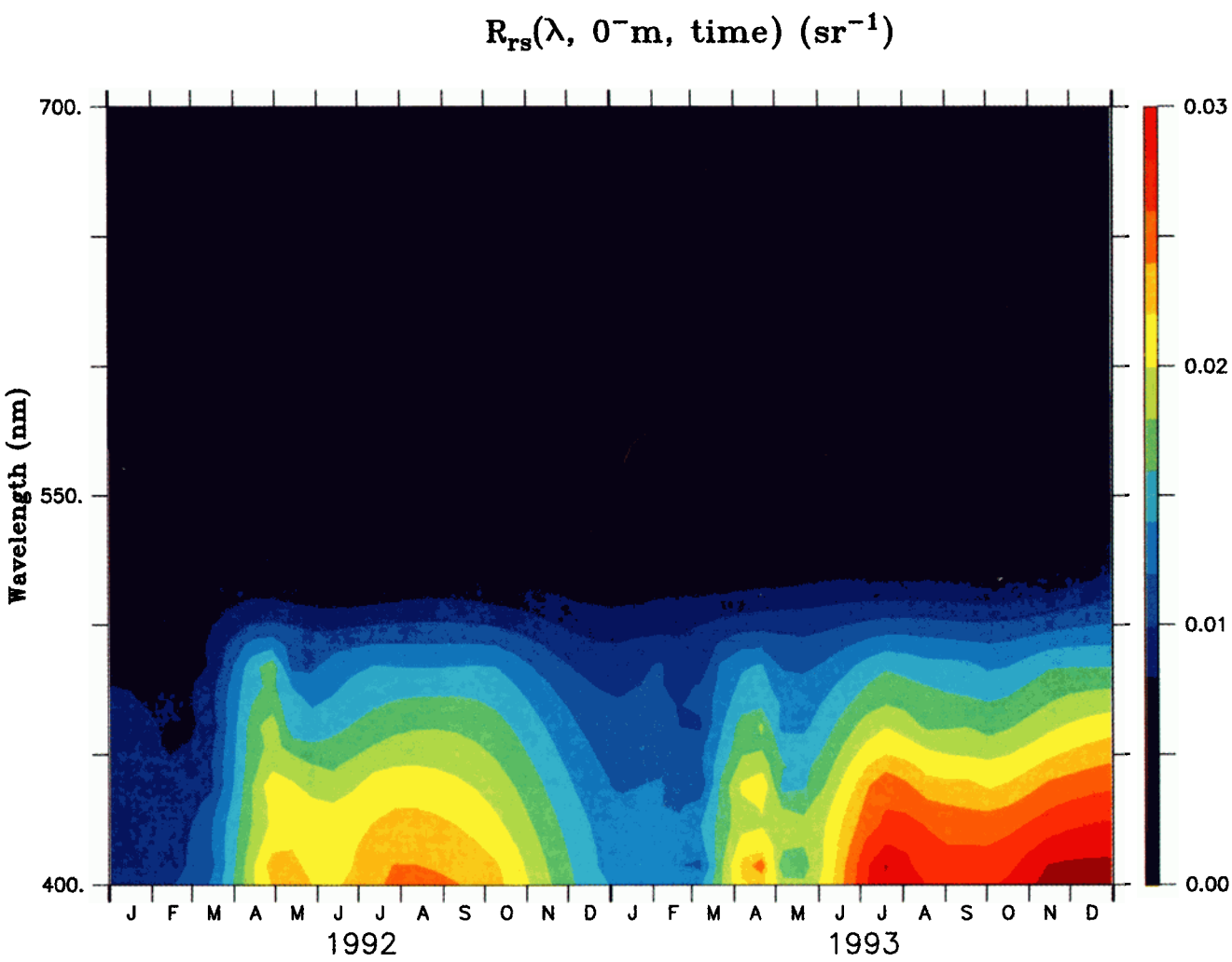

Plate 1. Bermuda Bio-Optics Project (BBOP) data; time series of remote-sensing reflectance spectra ($R_{rs}(0^-,\lambda)$) used as input to IOP inversion model (n=8 wavelengths). Units are in sr^{-1}.

particulate backscatter [e.g., *Morel*, 1987], are chosen. It is recognized that this conclusion may not hold for other oceanographic regions, in particular for case II waters.

The third model sensitivity analysis compares the four $a_{ph}^*(\lambda)$ spectra. The results of the linear regressions are again quite similar (Table 4). The *Garver et al.* [1994] and the *Bricaud et al.* [1995] $a_{ph}^*(\lambda)$ spectra result in the least number of negative $a_{dm}(441)$ retrievals for the summer-fall 1993 season (3% versus 15 to 19% for *Prieur and Sathyendranath* [1981] and *Morel* [1988], although statistically none of these retrieved negative values are significantly different than zero; Figure 5c). Varying the $a_{ph}^*(\lambda)$ spectra used as input to the IOP

Table 1b. Pearson's Correlation Coefficient of $R_{rs}(\lambda)$ Data Set

	$Fl_{chl\ a}$	$Fl_{chl\ a+pheo}$	$HPLC_{chl\ a}$	Nutrients	MLD	Bacteria	POC	PON	K_d(410:488)
R_{rs}(410)	-0.79*	-0.80*	-0.76*	-0.53*	0.51*	-0.17	-0.28	-0.56*	-0.87*
R_{rs}(441)	-0.81*	-0.81*	-0.79*	-0.53*	0.52*	-0.18	-0.24	-0.53*	-0.83*
R_{rs}(465)	-0.81*	-0.81*	-0.80*	-0.56*	0.49*	-0.17	-0.22	-0.49*	-0.79*
R_{rs}(488)	-0.79*	-0.79*	-0.79*	-0.57*	0.50*	-0.14	-0.14	-0.41*	-0.75*
R_{rs}(520)	-0.35*	-0.33	-0.37*	-0.35*	0.12	-0.18	-0.07	-0.14	-0.41*
R_{rs}(565)	0.13	0.13	0.10	0.09	-0.13	-0.12	-0.07	0.00	-0.09
R_{rs}(589)	0.17	0.17	0.14	0.03	-0.17	-0.08	-0.09	-0.04	0.00
R_{rs}(665)	0.19	0.23	0.17	0.00	-0.23	-0.03	-0.02	0.17	0.19

$R_{rs}(\lambda)$ data are remote-sensing reflectance at eight wave bands (nanometers).
*These correlation coefficients are significant at a level of 0.95.

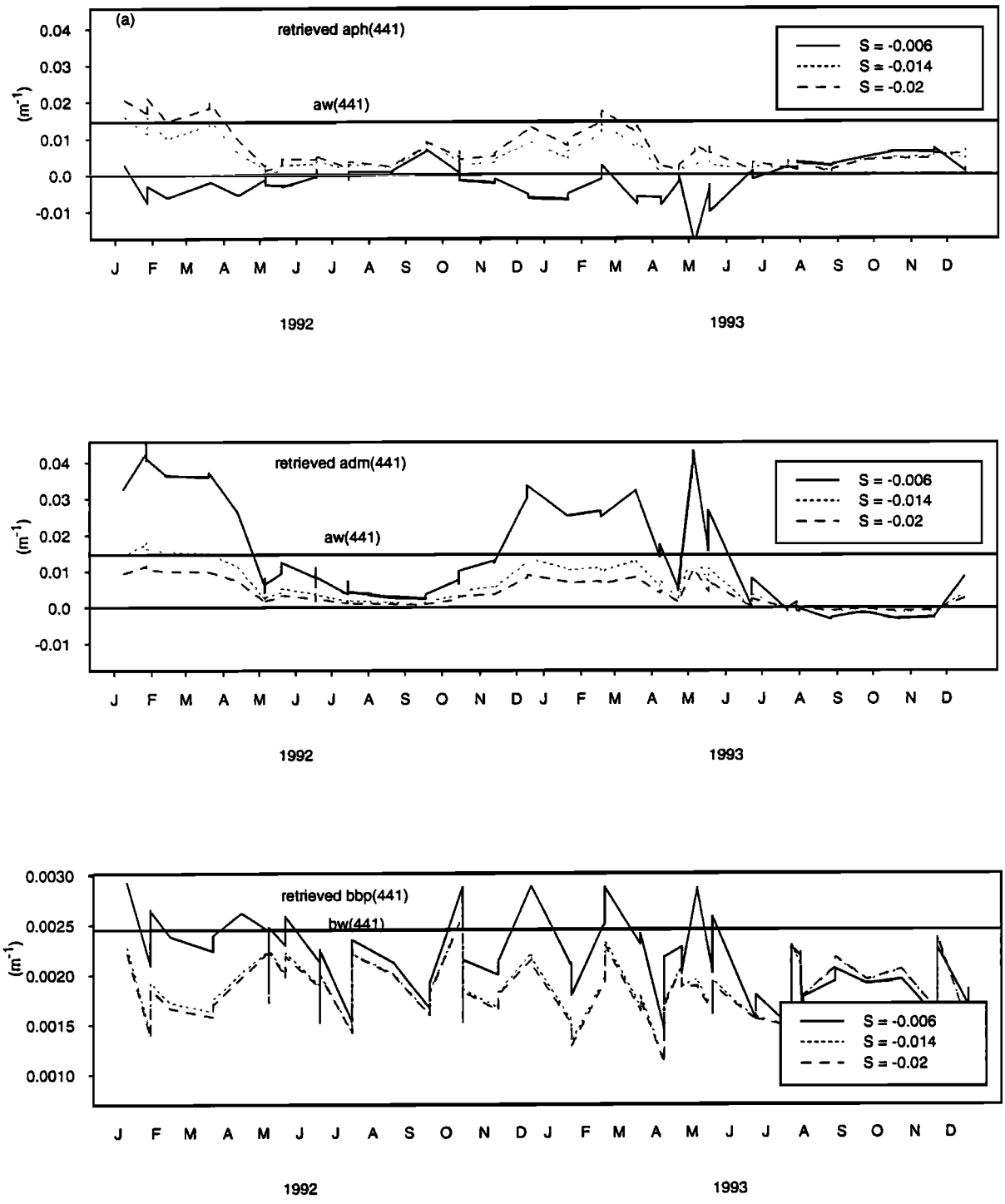

Figure 5. Results of sensitivity analyses performed on the IOP inversion model to assess the effects of varying the assumed spectral shape components. The three retrieved IOPs are the absorption coefficient due to phytoplankton ($a_{ph}(441)$), the absorption coefficient due to colored dissolved and detrital material ($a_{dm}(441)$), and the backscattering coefficient due to particulates ($b_{bp}(441)$). (a) Model set 1: three $a_{dm}^*(\lambda)$ spectra (S = -0.006, -0.014, -0.02 nm^{-1}) are each applied to the entire data set while holding the $a_{ph}^*(\lambda)$ and $b_{bp}^*(\lambda)$ spectra constant as *Morel* [1988] and λ^{-1}, respectively. (b) Model set 2: three $b_{bp}^*(\lambda)$ spectra (λ^0,λ^{-1},λ^{-2}) are each applied to entire data set while holding the $a_{dm}^*(\lambda)$ and $a_{ph}^*(\lambda)$ spectra constant as S equal to -0.02 nm^{-1} and *Morel* [1988], respectively. (c) Model set 3: four $a_{ph}^*(\lambda)$ spectra [*Prieur and Sathyendranath*, 1981; *Morel*, 1988; *Garver et al.*, 1994; *Bricaud et al.*, 1995] (P&S81, M88, G94, and B95) are each applied to entire data set while holding the $a_{dm}^*(\lambda)$ and $b_{bp}^*(\lambda)$ spectra constant as S equal to -0.02 nm^{-1} and λ^{-1}, respectively. (d) Final Sargasso Sea version of the IOP inversion model composed of the CDM specific absorption coefficient, modeled with S = -0.02 nm^{-1}, the modeled phytoplankton specific absorption coefficient of *Bricaud et al.* [1995], and the particulate specific backscattering coefficient modeled as λ^{-1}. Point estimates of the retrieved IOPs are shown along with 95% confidence intervals.

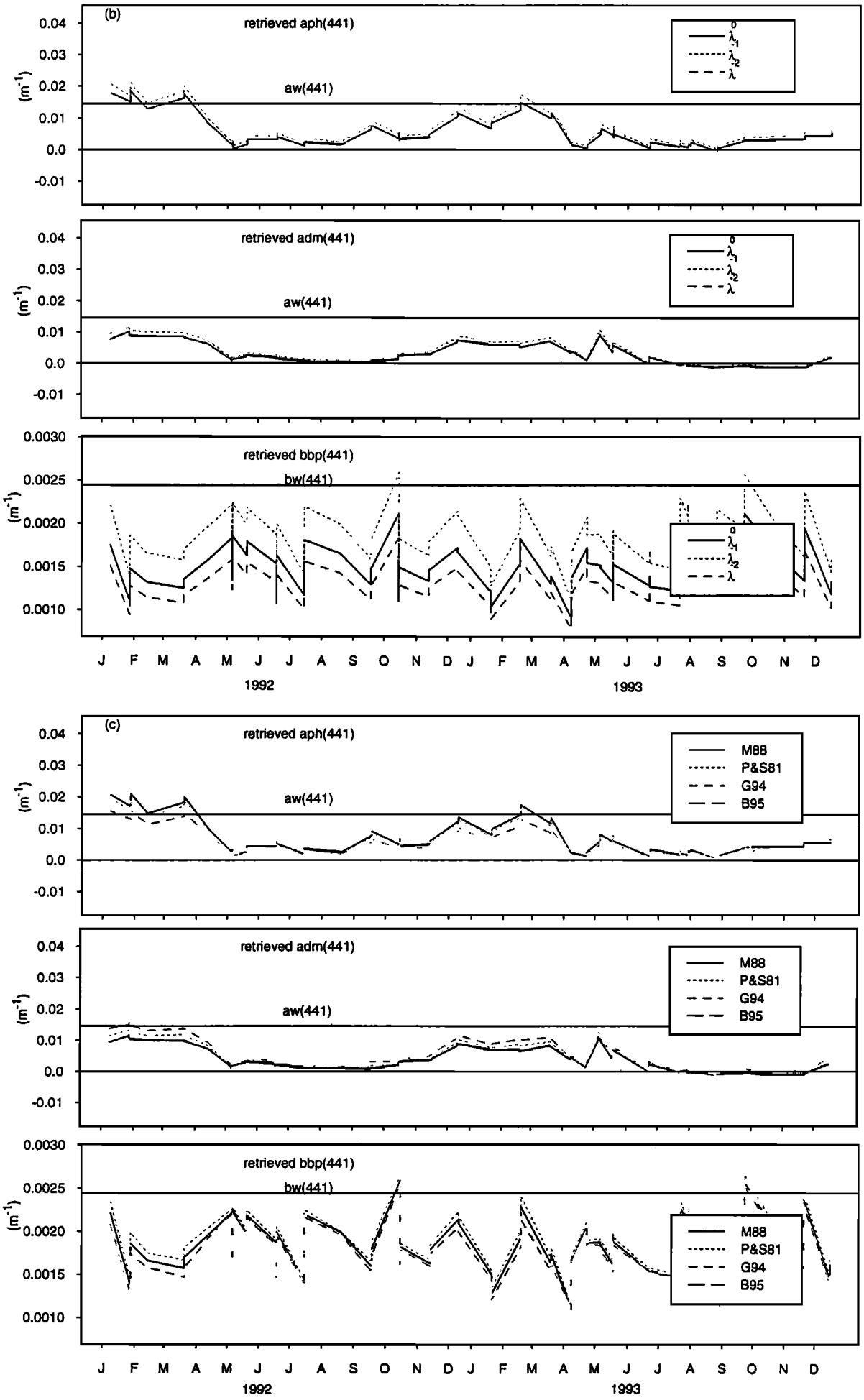

Figure 5. (continued)

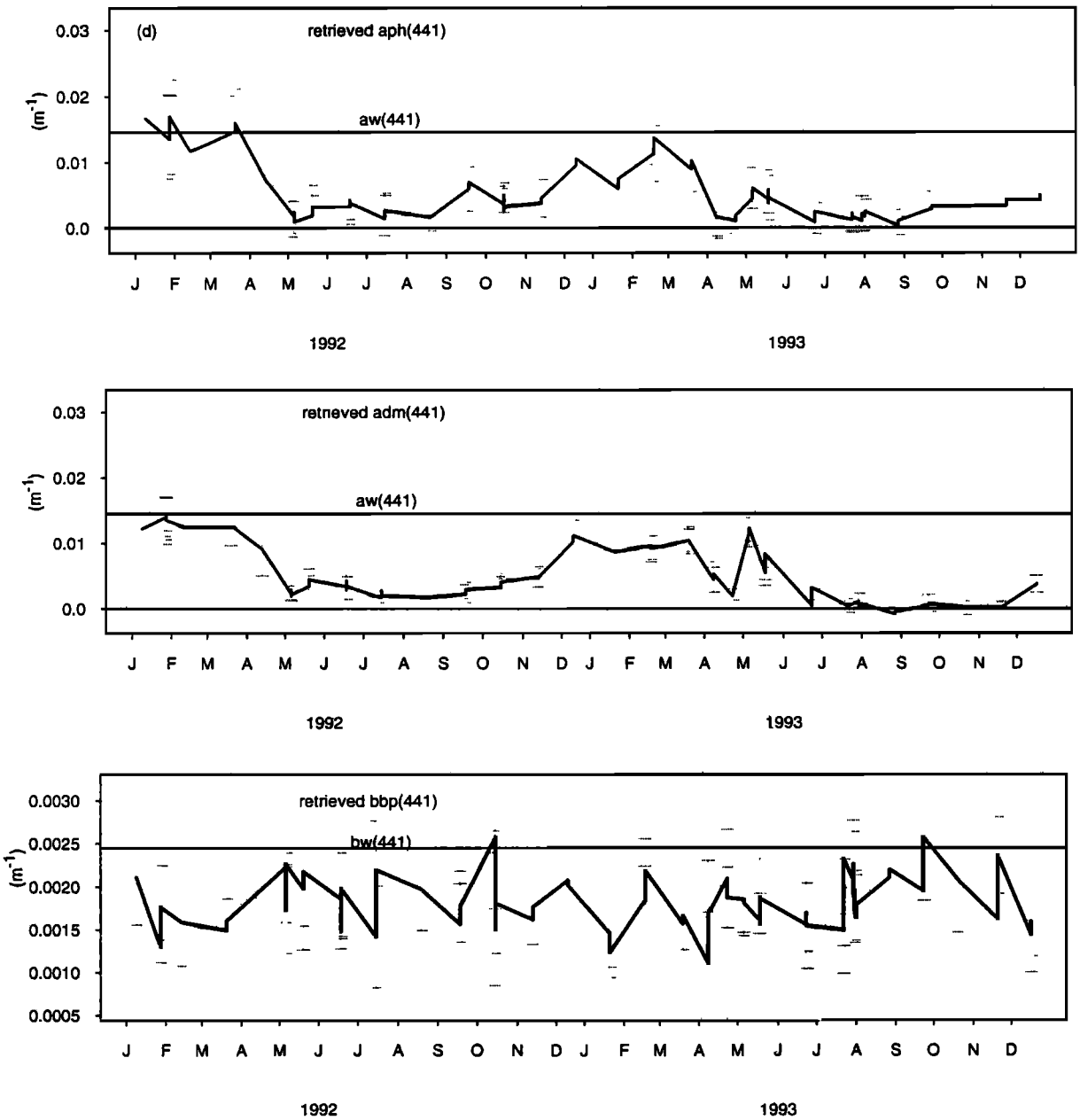

Figure 5. (continued)

Table 2. Results of Linear Regressions (Percent Variance Explained, r^2) Between Retrieved IOPs ($a_{ph}(441)$, $a_{dm}(441)$, and $b_{bp}(441)$) and BATS Biogeochemical Variables for Sensitivity Analysis Varying $a_{dm}^*(\lambda)$ Spectra

	S = -0.006 nm^{-1}			S = -0.014 nm^{-1}			S = -0.020 nm^{-1}		
	$a_{ph}(441)$	$a_{dm}(441)$	$b_{bp}(441)$	$a_{ph}(441)$	$a_{dm}(441)$	$b_{bp}(441)$	$a_{ph}(441)$	$a_{dm}(441)$	$b_{bp}(441)$
$Fl_{chl\ a}$	18	71	32	65	71	0	79	71	0
$Fl_{chl\ a+pheo}$	18	71	37	63	71	0	77	71	0
$HPLC_{chl\ a}$	12	68	27	73	68	0	84	68	1
$K_d(410{:}488)$	46	75	37	20	75	2	39	75	4
POC	22	6	5	2	6	0	0	6	0
PON	33	32	22	4	32	0	12	32	0
Nutrients	17	42	6	32	40	3	38	40	4
MLD	3	25	14	32	26	2	39	26	0
Bacteria	7	2	0	1	2	2	0	2	2

Here, λ^{-1} and *Morel* [1988] are held as constant.

Table 3. Results of Linear Regressions (Percent Variance Explained; r^2) Between Retrieved IOPs ($a_{ph}(441)$, $a_{dm}(441)$, and $b_{bp}(441)$) and BATS Biogeochemical Variables for Sensitivity Analysis Varying $b_{bp}^*(\lambda)$ Spectra as $(\lambda/\lambda_o)^{-n}$ (n = 0, 1 , 2)

	n = 0			n = 1			n = 2		
	$a_{ph}(441)$	$a_{dm}(441)$	$b_{bp}(441)$	$a_{ph}(441)$	$a_{dm}(441)$	$b_{bp}(441)$	$a_{ph}(441)$	$a_{dm}(441)$	$b_{bp}(441)$
$Fl_{chl\ a}$	78	70	2	79	71	0	78	70	2
$Fl_{chl\ a+pheo}$	77	69	2	77	71	0	77	69	2
$HPLC_{chl\ a}$	84	67	3	84	68	1	84	67	3
$K_d(410{:}488)$	39	76	8	39	75	4	39	76	8
POC	0	6	0	0	6	0	0	6	0
PON	12	32	0	12	32	0	12	32	0
Nutrients	39	41	7	38	40	4	39	41	7
MLD	39	25	0	39	26	0	39	25	0
Bacteria	0	2	2	0	2	2	0	2	2

Here S = -0.020 and *Morel* [1988] are held as constant.

model results in only minor changes in retrievals of either $a_{ph}(441)$ or $a_{dm}(441)$ and even less of a change in retrievals of $b_{bp}(441)$. As with the second model set, retrievals of $a_{ph}(441)$ are approximately equal to or greater than the value of $a_w(441)$ during the winter and early spring, while the retrievals of $a_{dm}(441)$ are approximately equal to the value of $a_w(441)$ during the winter and early spring. The $b_{bp}(441)$ retrievals are less than or equal to the value of $b_{bw}(441)$ throughout the time series. The *Bricaud et al.* [1995] model is chosen to continue with the sensitivity analysis as it results in very few negative retrievals of $a_{dm}(\lambda)$ and it allows for variations in the $a_{ph}^*(\lambda)$ spectra due to changes in pigment composition and packaging.

4.3. Final IOP Model

The IOP model is found to be most sensitive to changes in the $a_{dm}^*(\lambda)$ spectra, with some variability in model results seen when varying the $a_{ph}^*(\lambda)$ spectra and minimal variability observed using the different $b_{bp}^*(\lambda)$ spectra. The final version of the IOP inversion model is composed of the CDM specific absorption coefficient, modeled with S = -0.02 nm^{-1}, the modeled phytoplankton specific absorption coefficient of *Bricaud et al.* [1995], and the particulate specific backscattering coefficient modeled as λ^{-1}. The point estimates of the retrieved IOPs from this final model are shown in figure 5d, along with their 95% confidence intervals. The linear regressions between the final model IOPs and the BATS biogeochemical variables are shown in the last three columns of Table 4.

The average seasonal changes in the $a_{ph}(441)$ and $a_{dm}(441)$ retrievals are greater than their respective confidence intervals, indicating the significance of the temporal changes observed. The confidence intervals also demonstrate that the majority of the $a_{ph}(441)$ and many of the $a_{dm}(441)$ retrievals for the winter to late spring (December-March) are greater than or equal to $a_w(441)$ and that the two negative $a_{dm}(441)$ retrievals from summer 1993 are not significantly different than zero. There are no significant temporal changes observed in the $b_{bp}(441)$ retrievals, and the values for this IOP are consistently smaller than or equal to $b_{bw}(441)$ throughout the entire time series.

The retrieved $a_{ph}(441)$ values from the final model show a strong seasonal cycle and explain ~77% of the total variance in the BATS fluorometric pigment determinations and 84% of the HPLC chlorophyll *a* (last three columns of Table 4). The

Table 4. Results of Linear Regressions (Percent Variance Explained; r^2) Between Retrieved IOPs ($a_{ph}(441)$, $a_{dm}(441)$, and $b_{bp}(441)$) and BATS Biogeochemical Variables for Sensitivity Analysis Varying $a_{ph}^*(\lambda)$ Spectra.

	Morel [1988]			*Prieur and Sathyendranath* [1981]			*Garver et al.* [1994]			*Bricaud et al.* [1995]		
	$a_{ph}(441)$	$a_{dm}(441)$	$b_{bp}(441)$	$a_{ph}(441)$	$a_{dm}(441)$	$b_{bp}(441)$	$a_{ph}(441)$	$a_{dm}(441)$	$b_{bp}(441)$	$a_{ph}(441)$	$a_{dm}(441)$	$b_{bp}(441)$
$Fl_{chl\ a}$	79	71	0	78	75	0	79	78	3	79	78	3
$Fl_{chl\ a+pheo}$	77	71	0	77	75	0	77	77	3	77	77	3
$HPLC_{chl\ a}$	84	68	1	83	73	0	84	76	3	84	76	3
$K_d(410{:}488)$	39	75	4	38	73	3	40	70	8	40	70	8
POC	0	6	0	0	4	0	0	3	0	0	3	0
PON	12	32	0	12	30	0	12	28	0	12	28	0
Nutrients	38	40	4	38	41	3	38	41	7	38	41	7
MLD	39	26	0	39	29	1	39	32	0	39	32	0
Bacteria	0	2	2	0	1	2	0	1	2	0	1	2

Here S = -0.02 and λ^{-1} are held as constant.

magnitude of the spring bloom shown for 1992 is stronger than that seen in 1993 (Figure 5d). This is consistent with the changes in the nitrate+nitrite concentrations seen for this time period, suggesting a higher convective flux of nutrients into the euphotic zone for 1992 than for 1993 (Figure 4a). The retrieved $a_{dm}(441)$ values also show a strong seasonal cycle and explain ~77% of the variance in the pigment determinations and 70% of the variance in the ratios of $K_d(410)$ to $K_d(488)$. Time periods of high $a_{dm}(441)$ retrievals correspond to periods of deep mixing, causing dissolved and detrital materials to be brought to the surface. Time periods of low $a_{dm}(441)$ correspond to shallow mixing, perhaps resulting in photobleaching of colored dissolved and detrital material trapped at shallower depths. This pattern is also illustrated in the seasonal variability of $K_d(410)$ to $K_d(488)$ (Figure 3b). The nonseasonality observed in the retrieved $b_{bp}(441)$ values from the final model is reflected in the lack of coincidence between this parameter and any of the BATS biogeochemical variables.

To evaluate model performance, the residuals from the final model are examined to determine constant variance and a normal distribution. Small departures from normality do not affect the model greatly, but gross nonnormality is potentially serious as calculated model statistics and confidence intervals depend on the normality assumption. A normal probability plot of the IOP model residuals indicates they are normally distributed, while a plot of the fitted values versus the individual residuals shows near-constant variance with no unusual outliers (figures not shown). A plot of the spectrally summed root mean squared error (RMS_E) versus time shows an annual cycle, with larger RMS_E in the summer than in the winter months (Figure 6). This demonstrates that for this data set, the IOP model fits the in situ $R_{rs}(\lambda)$ spectra better in the winter, during conditions of higher pigment and CDM concentrations, than during the "blue" water conditions of the summer months. This suggests that our knowledge of "pure" seawater optical properties or our blue water optical parameterizations may still need improvement.

5. Discussion

We have shown that a statistically based ocean color inversion approach can be successfully applied in the blue ocean. These results give insights into what can be determined from space using ocean color spectra and how they relate to biogeochemical processes. To further evaluate the final IOP inversion model we (1) assess its capabilities as a chlorophyll *a* model, (2) examine the temporal changes in the retrieved estimates of CDM absorption, (3) assess the modeling and potential sources of the particulate backscatter coefficient, and (4) evaluate the application of the IOP model to satellite ocean color imagery, such as from the upcoming SeaWiFS and OCTS missions.

5.1. The IOP Model as a Chlorophyll Model

One of the primary goals of the SeaWiFS mission is to provide global coverage of chlorophyll *a* concentrations to within an accuracy of 35% [*Hooker et al.*, 1992]. As the final IOP model is developed using only existing globally applicable bio-optical models, it can potentially provide global estimates of chlorophyll *a* concentrations. The retrieved chlorophyll *a* estimates from the final IOP model show excellent correspondence in a linear regression with the BATS HPLC chlorophyll *a* determinations (r^2 = 81%; Figure 7a). This result can be compared with chlorophyll estimates obtained from a band ratio or CZCS-type pigment algorithm of the form [*Gordon and Morel*, 1983]

$$CZCS_{chl} = A * \frac{L_u(\lambda_1)^B}{L_u(\lambda_2)} \tag{8}$$

where $CZCS_{chl}$ is the band ratio estimated chlorophyll concentration (milligrams per cubic meter), $L_u(\lambda)$ is the upwelled radiance, λ_1 = 441 nm, λ_2 = 565 nm, A = 1.92 mg m^{-3}, and B = -1.80.

The results of the two models are quite similar, with the CZCS chlorophyll estimates explaining 86% of the variance in the BATS HPLC chlorophyll *a* determinations. Other CZCS band ratio models yielded similar results [*Gordon and Morel*, 1983]. When evaluated by season, the two models perform markedly better in the winter (r^2 = 73 to 94%), when chlorophyll *a* values are highest, than during the summer season (r^2 = 1 to 15%). Importantly, the IOP model chlorophyll *a* estimates have a clearer 1:1 relationship with the BATS HPLC chlorophyll *a* values, as is indicated by a slope of 0.97 (intercept = 0.033 mg m^{-3}). In contrast, the CZCS regression has a slope of 1.75 (intercept = -0.005 mg m^{-3}). This underestimate of the BATS HPLC chlorophyll *a* values by the CZCS algorithm is particularly apparent in the winter-spring months (Figure 7b), whereas the IOP model chlorophyll *a* estimates more closely approximate the

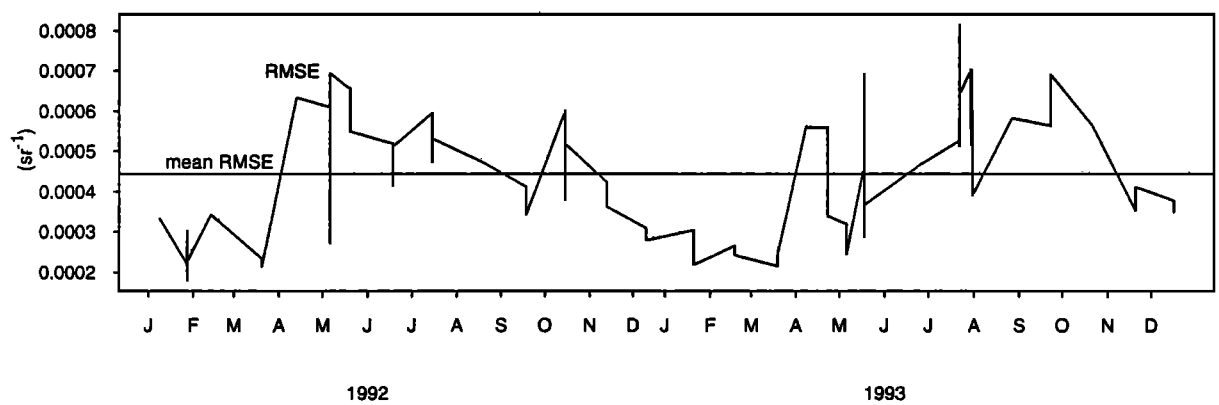

Figure 6. Time series of spectrally summed root mean squared error (RMS_E) from final Sargasso Sea IOP inversion model.

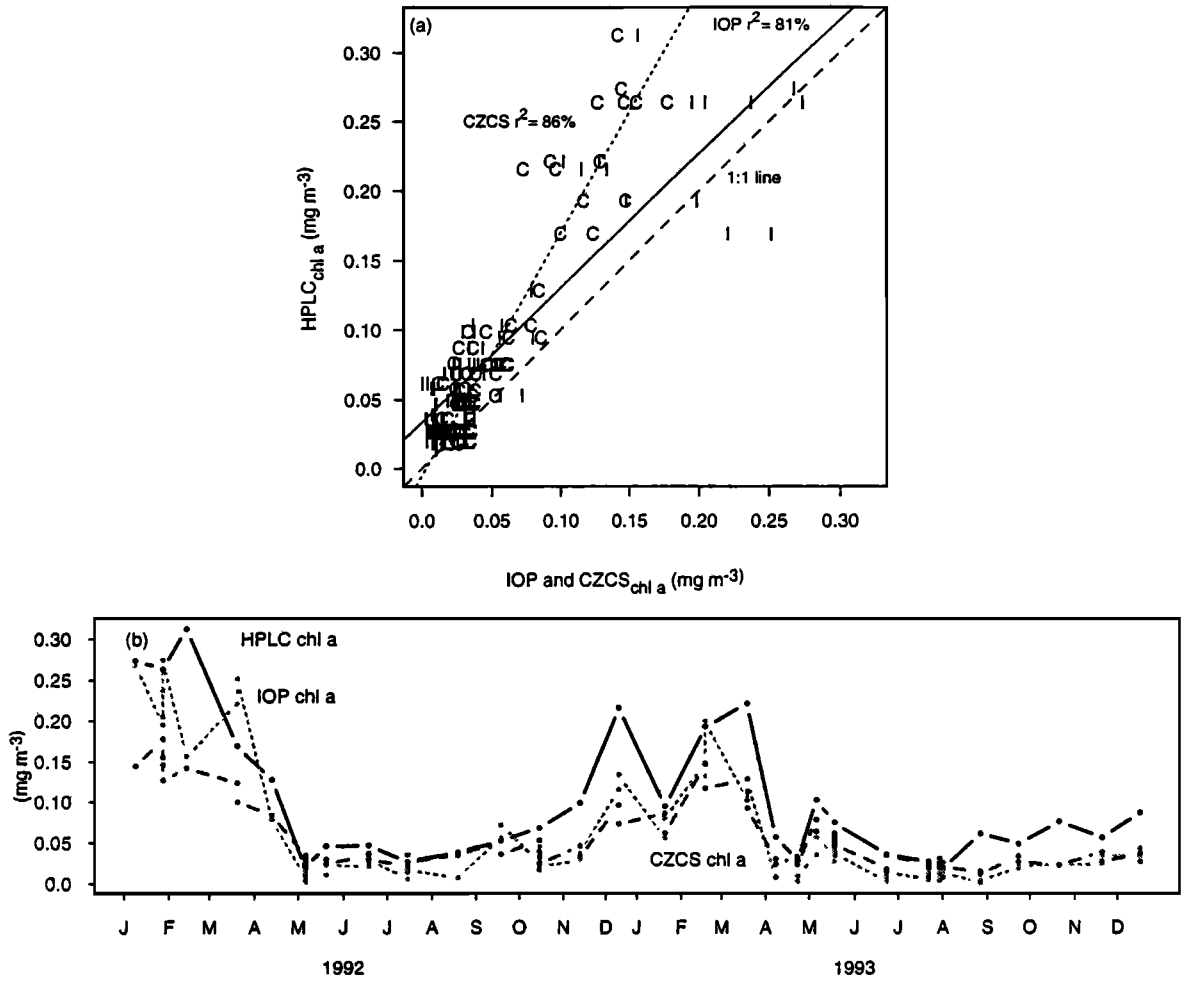

Figure 7. (a) Results of linear regressions between BATS HPLC chlorophyll *a* determinations and the estimated chlorophyll *a* concentrations from the IOP inversion model (r^2 = 81%) and a CZCS band ratio chlorophyll algorithm (r^2 = 86%). Units are milligrams per cubic meter. (b) Time series of BATS HPLC chlorophyll *a* determinations and estimated chlorophyll *a* concentrations from the IOP inversion model and a CZCS band ratio chlorophyll algorithm. Units are milligrams per cubic meter.

magnitudes of the BATS HPLC chlorophyll *a* values. This is perhaps due to the IOP models ability to separate phytoplankton absorption from CDM absorption [*Carder et al.*, 1989; *Siegel and Michaels*, 1996]. The seasonal underestimate of chlorophyll *a* by the CZCS algorithm may be consistent with this idea. It should also be noted that the CZCS algorithm was not developed using very much blue water data [*Gordon and Morel*, 1983]. Hence this comparison with the "global" CZCS band ratio algorithm may not be fair using the present blue water data set. Another explanation for the difference in model results is that the empirical CZCS algorithm was developed with pigment data (fluorometric techniques) measured on GF/C filters, as opposed to the *Bricaud et al.* [1995] model used here which was developed with pigment data (HPLC techniques) on GF/F filters. GF/C filters have a higher porosity than GF/F filters, with a 15% underestimate of chlorophyll *a* using GF/C filters shown by Chavez *et al.* [1995].

5.2. Temporal Changes in CDM Versus Total Absorption

As discussed previously, absorption by CDM appears to play an important role in affecting retrievals of chlorophyll *a* concentrations. The fraction of total absorption attributed to CDM is evaluated by examining the ratio of $a_{dm}(441)$ to $a_{tot}(441)$ retrievals from the final model (where $a_{tot}(441) = a_w(441) + a_{ph}(441) + a_{dm}(441)$). Seasonally, CDM absorption is shown to range from 0 to 35% at 441 nm and from 0 to 50% at 410 nm (Figure 8a). Higher CDM absorption is observed in the winter-spring months when deep mixed layer depths bringing colored dissolved and detrital materials to the surface, while CDM absorption is at a minimum in the summer-fall months when the mixed layer is shallowest and the water column is stratified [*Siegel et al.*, 1995a]. The temporal signal of absorption due to CDM is mirrored in the ratios of $K_d(410)$ to $K_d(488)$ (Figures 4b and 8b), which explain 86% of the variance in the ratios of $a_{dm}(441)$ to $a_{tot}(441)$. Accurate estimates of CDM absorption are important as its presence can confound estimates of chlorophyll *a* from ocean color spectra [e.g., *Siegel and Michaels*, 1996]. Further, the robust detection of CDM absorption gives a remotely sensed parameter which describes the concentration of colored decomposition products in the sea. It is yet unclear how this parameter may be used to make better predictions of ecosystem functions. However, it should be clear that seasonal changes in the rates of photochemistry should be affected by CDM absorption values [*Siegel and Michaels*, 1996].

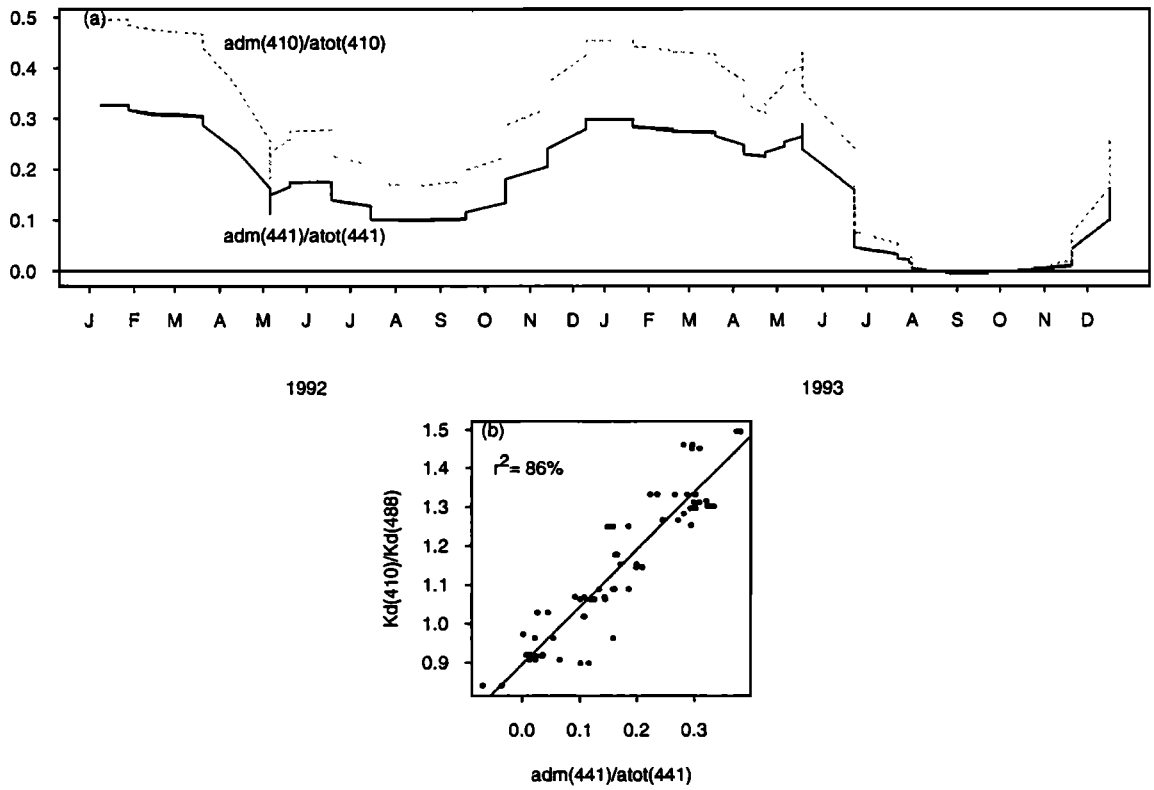

Figure 8. (a) Time series of ratios of $a_{dm}(410)$ to $a_{tot}(410)$ and $a_{dm}(441)$ to $a_{tot}(441)$. (b) Results of linear regression between $a_{dm}(441)$ to $a_{tot}(441)$ and $K_d(410)$ to $K_d(488)$ (r^2 = 86%).

5.3. Modeling of Particulate Backscatter

The modeled values of particulate backscatter for this data set have been shown to be smaller than or equal to values of backscatter by pure seawater and lacking any temporal signal, despite the significant seasonal chlorophyll *a* signal observed. This is inconsistent with several previous bio-optical models of particulate backscatter. For example, *Morel* [1988] models particulate backscatter as a weak function of the chlorophyll *a* concentration, or

$$b_{bp}(\lambda) = 0.30 Chl^{0.62}\left\{0.002 + 0.02(1/2 - 1/4 \log Chl)\left[\frac{550}{\lambda}\right]\right\} \quad (9)$$

where *Chl* is the chlorophyll *a* concentration (milligrams per cubic meter). This empirically derived model was developed for case I waters only with a λ^{-1} wavelength dependence for $b_{bp}(\lambda)$. For the range of BATS chlorophyll *a* concentrations observed (0.02 to 0.31 mg m^{-3}; Figure 3a) the average $b_{bp}(441)$ value calculated using this model is 0.0018 m^{-1}. This is in agreement with the average IOP model $b_{bp}(441)$ retrieval, which is also 0.0018 m^{-1}. A second estimate of $b_{bp}(441)$ uses the approximation of *Gordon et al.* [1988],

$$b_b(\lambda) \approx K_d(\lambda)/0.11 R_{rs}(\lambda) \quad (10)$$

where $K_d(\lambda)$ is averaged over the upper 20 m of the water column. Using this approximation, the average $b_{bp}(441)$ estimate is again consistent with the average IOP model $b_{bp}(441)$ retrieval at 0.0017 m^{-1}. Though all three $b_{bp}(441)$ estimates are quite similar in magnitude, the *Morel* [1988] backscatter model demonstrates a seasonal cycle as a function of chlorophyll *a*, while the other two models show no seasonal signal (figure not shown). In addition, none of the three particulate backscatter estimates are significantly correlated with one another. These varied results in estimates of $b_{bp}(\lambda)$ demonstrate how divergent the various current backscatter models are and the difficulty in accurately estimating this parameter.

While these roughly consistent retrievals of $b_{bp}(\lambda)$ demonstrate they are not related to changes in chlorophyll *a* concentration, they make no statement as to the other possible sources of the $b_{bp}(\lambda)$ signal. For example, bacterial abundance's have recently been implicated as a significant component of the particulate backscatter signal [*Stramski and Kiefer*, 1990, 1991; *Morel and Ahn*, 1991]. Values for backscatter due to bacteria, $b_{bbac}(\lambda)$, can be calculated using

$$b_{bbac}(\lambda) = N\pi \frac{\overline{D}^2}{4} Q_{bb}(\lambda, m, \overline{D}) \quad (11)$$

where N is the numerical abundance of bacteria observed at the BATS site (cells per cubic meter; Figure 4b), $\overline{D}$ is an average diameter of bacterial cells (micrometers), $Q_{bb}(\lambda, m, \overline{D})$ is the efficiency factor for backscattering, and m is the real part of the refractive index. Values of $\overline{D}$ observed at the BATS site range from 0.42 to 0.49 μm [*Carlson et al.*, 1996], and a typical range of $Q_{bb}(441)$ for bacteria from Mie calculations is $5 \cdot 10^{-4}$ to $2 \cdot 10^{-3}$ for refractive indices of m = 1.042 and 1.068 [*Stramski and Kiefer*, 1990]. The results of these calculations indicate that values of $b_{bbac}(441)$ could compose from 2 to 12% of the modeled $b_{bp}(441)$ retrievals.

A second estimate of the role of bacteria in particulate backscatter can be made based on the laboratory experiments of *Stramski and Kiefer* [1990], who measured a bacteria specific backscattering coefficient of $2.7 \cdot 10^{-16}$ m^2 $cell^{-1}$. Using the observed bacterial abundance's (Figure 4b), bacteria could contribute up to 9% of the IOP modeled particulate

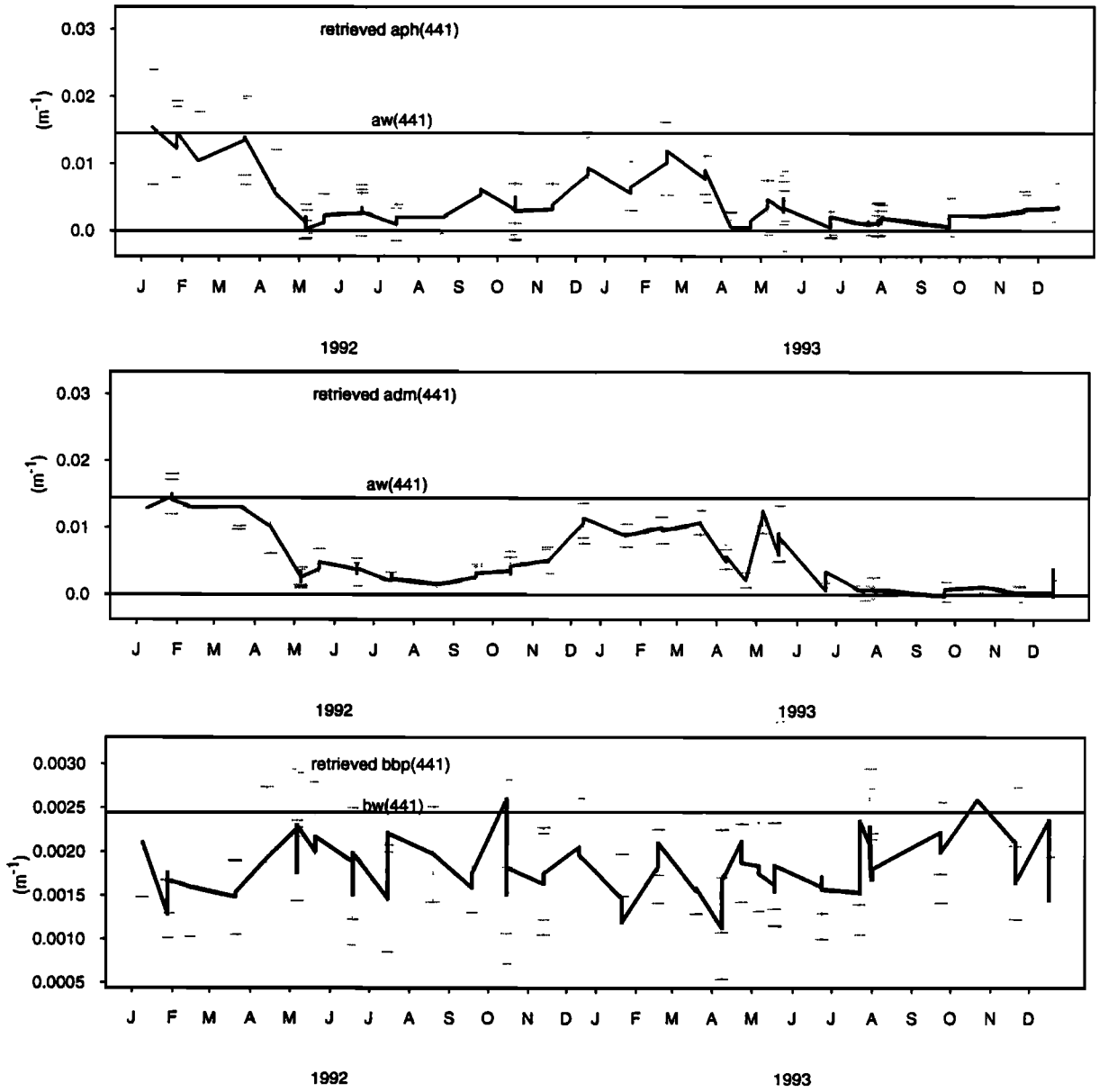

Figure 9. Results of the final version of the IOP inversion model using the six wavelengths that most closely match the sea viewing wide field of view sensor (SeaWiFS) wave bands minus the 670 nm atmospheric correction channel (n=5). Point estimates of the retrieved IOPs are shown along with 95% confidence intervals.

backscatter. These calculations are in general agreement with *Stramski and Kiefer* [1991] and *Morel and Ahn* [1991], who estimate that heterotrophic bacteria typically account for 5-20% of backscattering in oligotrophic waters. This suggests that other constituents besides heterotrophic bacteria must contribute the remainder of the $b_{bp}(\lambda)$ signal. These particles are likely to be inanimate particulates such as submicron size detrital particles as suggested by *Stramski and Kiefer* [1991]. This question remains unresolved at this time.

5.4. Application to Upcoming Satellite Ocean Color Missions

The final phase in the assessment of the IOP inversion model is its application to the next generation of ocean color satellite imagers such as the SeaWiFS mission. Importantly, only six visible wave bands will be available for SeaWiFS (412, 443, 490, 510, 555, and 670 nm [*Hooker et al.*, 1992]). In order to evaluate the application of the IOP model to SeaWiFS imagery, we use only the wave bands nearest those planned for SeaWiFS. Further, as the $R_{rs}(670)$ channel may be used for atmospheric correction [*Ding and Gordon*, 1995], it has been omitted from the analysis. The results of the SeaWiFS model are nearly identical to the final IOP model (Figure 9) with a change of only 1 to 6% in the linear regressions between the retrieved SeaWiFS IOPs and the BATS data set (Table 5 versus final model results in Table 4). In addition, the retrieved SeaWiFS IOPs and confidence intervals are virtually identical to the final IOP model results, which use all eight available wave bands (Figure 9 versus Figure 5d). This demonstrates the potential usefulness of applying the IOP model to future SeaWiFS imagery as a global case I

Table 5. Results of Linear Regressions (Percent Variance Explained; r^2) Between Retrieved IOPs ($a_{ph}(441)$, $a_{dm}(441)$, and $b_{bp}(441)$) and BATS Biogeochemical Variables for Final IOP Model Using SeaWiFS Wave Bands Minus 670 nm Atmospheric Correction Channel ($n = 5$)

	$a_{ph}(441)$	$a_{dm}(441)$	$b_{bp}(441)$
$Fl_{chl\ a}$	77	76	5
$Fl_{chl\ a+pheo}$	75	75	5
$HPLC_{chl\ a}$	86	76	6
$K_d(410{:}488)$	34	69	10
POC	2	3	0
PON	7	27	0
Nutrients	38	41	10
MLD	41	27	0
Bacteria	0	1	2

algorithm. A more comprehensive evaluation of its suitability as a global model is presently underway.

6. Conclusions and Summary

An inherent optical property inversion model for ocean color spectra has been successfully applied to data from the Sargasso Sea. Specifically, the IOP model retrieves estimates of absorption by phytoplankton, absorption by CDM, and backscatter by particulates, as opposed to the single chlorophyll *a* parameter so often retrieved using CZCS-type algorithms. The strong seasonal variations in ocean biogeochemistry observed in the Sargasso Sea, coupled with the suite of optical and biogeochemical data available through the BBOP and BATS programs, have afforded an excellent opportunity to develop and test the IOP inversion model.

The results of this study show that changes in the constituents that compose total absorption are primarily responsible for the temporal changes observed in $R_{rs}(\lambda)$. Most importantly, changes in the dissolved and detrital absorption properties are a more significant source of ocean color variability in the Sargasso Sea than changes in phytoplankton absorption. The retrieved $a_{ph}(441)$ and $a_{dm}(441)$ estimates show strong seasonal cycles and good correspondence with BATS pigment determinations and indicators of CDM concentration such as the ratio of $K_d(410)$ to $K_d(488)$. IOP model estimates of chlorophyll *a* concentrations compare well with those derived from standard band ratio algorithms, demonstrating its value as a chlorophyll *a* algorithm. Retrieved estimates of $a_{dm}(441)$ compose approximately 35% of the total absorption coefficient during the winter-spring season and 0 to 10% during the summer season. This illustrates the importance of estimating CDM absorption in conjunction with chlorophyll *a* concentrations, as the presence of CDM will obscure the chlorophyll *a* induced ocean color signal.

In contrast, retrieved estimates of particulate backscatter show no significant temporal variations. The retrieved $b_{bp}(441)$ values are typically smaller than $b_{bw}(441)$ for the entire time series and demonstrate no correspondence with any of the BATS variables. This indicates that $b_{bp}(\lambda)$ is, at best, weakly affected by chlorophyll containing particles. Bacteria are shown to contribute up to 10% to estimates of particulate backscatter, in agreement with both *Stramski and Kiefer* [1991] and *Morel and Ahn* [1991]. This illustrates that other constituents besides bacteria must contribute to $b_{bp}(\lambda)$.

The long-range goal of this work is to apply the IOP inversion model to remotely sensed ocean color imagery, such as from the upcoming SeaWiFS and OCTS satellite missions. It is recognized here that while modeling CDM absorption using an exponential decay constant of 0.02 nm^{-1} may hold for the blue Sargasso Sea, it is by no means a global constant. The fact that the exponential decay constant is the greatest source of variability in the IOP model and that it varies both spatially and temporally will necessitate the reconfiguration of the IOP model to retrieve the exponential decay constant, *S*, as a parameter. This is something that we are presently investigating. The ability to successfully retrieve accurate estimates of $a_{ph}(441)$, $a_{dm}(441)$, $b_{bp}(441)$ (and in the future *S*) from ocean color imagery will provide new parameters so that basin scale estimates of biological processes, such as phytoplankton distributions, primary production rates, and biogenic gas fluxes, can be successfully modeled from space.

Notation

λ wavelength, nm.
λ_o reference wavelength (= 440), nm.
$a(\lambda)$ total absorption coefficient, m^{-1}.
$b(\lambda)$ total scattering coefficient, m^{-1}.
$b_b(\lambda)$ total backscattering coefficient, m^{-1}.
$R_{rs}(\lambda)$ remote sensing reflectance (= $L_u(\lambda)/E_d(\lambda)$, sr^{-1}.
$L_u(\lambda)$ upwelling radiance, W sr^{-1} m^{-2} nm^{-1}.
$E_d(\lambda)$ downwelling irradiance, W m^{-2} nm^{-1}.
$a_w(\lambda)$ absorption coefficient for pure seawater, m^{-1}.
$b_{bw}(\lambda)$ backscattering coefficient for pure seawater, m^{-1}.
$a_{ph}(\lambda)$ absorption coefficient for phytoplankton, m^{-1}.
$a_{dm}(\lambda)$ absorption coefficient for dissolved/detrital materials, m^{-1}.
$b_{bp}(\lambda)$ backscattering coefficient for particulates, m^{-1}.
Chl chlorophyll concentration, mg m^{-3}.
$a_{ph}^*(\lambda)$ $a_{ph}(\lambda)/Chl$, m^2 mg^{-1}.
$a_{dm}^*(\lambda)$ $a_{dm}(\lambda)/a_{dm}(\lambda_o)$.
$b_{bp}^*(\lambda)$ $b_{bp}(\lambda)/b_{bp}(\lambda_o)$.
l_1 constant = 0.0949, sr^{-1}.
l_2 constant = 0.0794, sr^{-1}.
$b_m^{sw}(\lambda)$ total scattering by seawater, m^{-1}.
S exponential decay constant, nm^{-1}.
Y_n responses (equal to $R_{rs}(\lambda_n)$) from nonlinear model, sr^{-1}.
$f(x_n, \theta_p)$ nonlinear model expectation function (equal to $\hat{R}_{rs}(\lambda_n)$), sr^{-1}.
n index of realization per observation (total of eight wavelengths).
x_n matrix of independent variables from nonlinear model .
θ_p array of unknown parameters from nonlinear model .
Z_n residuals from nonlinear model, sr^{-1}.
$a_{ph}(441)$ modeled absorption coefficient for phytoplankton (equal to $Chl\ a_{ph}^*(441)$), m^{-1}.
$a_{dm}(441)$ modeled absorption coefficient for CDM (equal to $a_{dm}(\lambda_o)$ $a_{dm}^*(441)$), m^{-1}.
$b_{bp}(441)$ modeled backscattering coefficient for particulates (equal to $b_{bp}(\lambda_o)$ $b_{bp}^*(441)$), m^{-1}.
σ_e standard errors from nonlinear model.
$k_d(\lambda)$ diffuse attenuation coefficient, m^{-1}.
$CZCS_{chl}$ chlorophyll estimates from CZCS pigment algorithm.
A constant = 1.92, mg m^{-3}.
B constant = -1.80.
$a_{tot}(441)$ $a_w(441) + a_{ph}(441) + a_{dm}(441)$, m^{-1}.
$b_{bbac}(\lambda)$ backscattering coefficient due to bacteria, m^{-1}.
N numerical abundance of bacteria observed at BATS site, cells m^{-3}.
$\overline{D}$ average diameter of bacterial cells, mm.
Q_{bb} efficiency factor for backscattering.
m real part of the refractive index (= 1.042 and 1.068).

Acknowledgments. This work was supported by the NASA Global Change Fellowship Program (NGT-300141). Funding for the BBOP program is provided by NASA (NAGW-3145), the SeaWiFS project office (NCC-5-49), and NSF (OCE 91-16372 and OCE 90-16990). NSF also supports the core BATS program (OCE 88-01089, OCE 93-01950). The authors would like to thank all the field technicians involved in the BATS/BBOP programs for their excellent work in developing the quality data sets presented here. In particular, we gratefully acknowledge Melodie Hammer and Liz Caporelli for their dedication and hard work in the implementation and maintenance of the BBOP program at the Bermuda Biological Station for Research. Margaret O'Brien provides the processing and quality control of the BBOP data set. Dave Menzies performs the quarterly calibrations of the BBOP radiometer. Discussions with Tony Michaels, Jens Sorensen, Margaret O'Brien, Craig Carlson, Norm Nelson, Joel Michaelsen, and Doug Bates, as well as comments from the reviewers, have been extremely helpful.

References

Morel, A., Optical properties of pure wAhn, Y., A. Bricaud, and A. Morel, Light backscattering efficiency and related properties of some phytoplanktors, *Deep Sea Res., Part A, 39*, 1835-1855, 1992.

Balch, W. M., P. M. Holligan, S. G. Ackleson, and K. J. Voss, Biological and optical properties of mesoscale coccolithophore blooms in the Gulf of Maine, *Limnol. Oceanogr., 36*(4), 629-643, 1991.

Bates, D. M., and D. G. Watts, *Nonlinear Regression Analysis and Its Applications*, John Wiley, New York, 1988.

Bricaud, A., A. Morel, and L. Prieur, Optical efficiency factors of some phytoplanktors, *Limnol. Oceanogr., 28*(5), 816-832, 1983.

Bricaud, A., M. Babin, A. Morel, and H. Claustre, Variability in the chlorophyll-specific absorption coefficients of natural phytoplankton: Analysis and parameterization, *J. Geophys. Res., 100*(C7), 13,321-13,332, 1995.

Carder, K. L., R. G. Steward, G. R. Harvey, and P. B. Ortner, Marine humic and fulvic acids: Their effects on remote sensing of ocean chlorophyll, *Limnol. Oceanogr., 34*(1), 68-81, 1989.

Carder, K. L., S. K. Hawes, K. S. Baker, R. C. Smith, R. G. Steward, and B. G. Mitchell, Reflectance model for quantifying chlorophyll *a* in the presence of productivity degradation products, *J. Geophys. Res., 96*(C11), 20,599-20,611, 1991.

Carlson, C. A., H W. Ducklow, and T. D. Sleeter, Stocks and dynamics of Bacterioplankton in the Northwestern Sargasso Sea, *Deep Sea Res., Part II, 43*, 491-515, 1996.

Chavez, F. P., *et al.*, On the chlorophyll *a* retention properties of glass fiber GF/F filters, *Limnol. Oceanogr., 40*(2), 428-433, 1995.

Dickey, T. D., The emergence of concurrent high-resolution physical and bio-optical measurements in the upper ocean and their applications, *Rev. Geophys., 29*(3), 383-413, 1991.

Ding, K.Y., and H. R. Gordon, Analysis of the influence of O_2 a-band absorption on atmospheric correction of ocean-color imagery, *Appl. Opt.*, 34, 2068-2080, 1995.

Garver, S. A., D. A. Siegel, and B. G. Mitchell, Variability in near-surface particulate absorption spectra: What can a satellite ocean color imager see?, *Limnol. Oceanogr., 39*(6), 1349-1367, 1994.

Gordon, H. R., and K. Y. Ding, Self-shading of in-water optical instruments, *Limnol. Oceanogr., 37*(3), 491-500, 1992.

Gordon, H. R., and A. Morel, *Remote Assessment of Ocean Color for Interpretation of Satellite Visible Imagery: A review*, Springer-Verlag, New York, 1983.

Gordon, H. R., O. B. Brown, R. H. Evans, J. W. Brown, R. C. Smith, K. S. Baker, and D. K. Clark, A semianalytic radiance model of ocean color, *J. Geophys. Res., 93*(D9), 10,909-10,924, 1988.

Green, S. A., and N. V. Blough, Optical absorption and fluorescence properties of chromophoric dissolved organic matter in natural waters, *Limnol. Oceanogr., 39*(8), 1903-1916, 1994.

Hooker, S. B., W. E. Esaias, G. C. Feldman, G. W. Watson and C. R. McClain, An overview of SeaWiFS and ocean color, edited by S. B. Hooker and E. R. Firestone, *NASA Tech. Memo. 104566*, vol. 1, 24 pp., 1992.

Kirk, J. T. O., *Light and Photosynthesis in Aquatic Ecosystems*, Cambridge University Press, New York, 1994.

Kishino, M., C. R. Booth, and N. Okami, Underwater radiant energy absorbed by phytoplankton, detritus, dissolved organic matter, and pure water, *Limnol. Oceanogr., 29*(2), 340-347, 1984.

Kitchen, J. C., and J. R. V. Zaneveld, On the noncorrelation of the vertical structure of light scattering and chlorophyll *a* in case I waters, *J. Geophys. Res., 95*(C11), 20,237-20,246, 1990.

Knap, A. H., et al., *BATS Methods-March 1993, BATS Method Manual Version 3*, 108 pp., U. S. Joint Global Ocean Flux Study Plann. and Coord. Off., Woods Hole, Mass., 1993.

Menzel, D. W., and J. H. Ryther, The annual cycle of primary production in the Sargasso Sea off Bermuda, *Deep Sea Res., 6*, 351-367, 1960.

Menzel, D. W., and J. H. Ryther, Annual variations in primary production of the Sargasso Sea off Bermuda, *Deep Sea Res., 7*, 282-288, 1961.

Michaels, A. F., et al., Seasonal patterns of ocean biogeochemistry at the US-JGOFS Bermuda Atlantic Time Series Study site, *Deep Sea Res., Part I, 41*, 1013-1036, 1994.

Mitchell, B. G., Coastal zone color scanner retrospective, *J. Geophys. Res., 99*(C4), 7291-7292, 1994.

Morel, A., Optical properties of pure water and pure seawater, in *Optical Aspects of Oceanography*, edited by N. G. Jerlov and E. S. Nielsen, pp. 1-24, Academic Press, San Diego, Calif., 1974.

Morel, A., Chlorophyll-specific scattering coefficient of phytoplankton: A simplified theoretical approach, *Deep Sea Res., Part A, 34*, 1093-1105, 1987.

Morel, A., Optical modeling of the upper ocean in relation to its biogenous matter content (case I waters), *J. Geophys. Res., 93*(C9), 10,749-10,7681988.

Morel, A., and Y. Ahn, Optics of heterotrophic nanoflagellates and ciliates: A tentative assessment of their scattering role in oceanic waters compared to those of bacterial and algal cells, *J. Mar. Res., 49*(1), 177-202, 1991.

Morel, A., and L. Prieur, Analysis of variations in ocean color, *Limnol. Oceanogr., 22*(4), 709-722, 1977.

Morrow, J. H., D. A. Kiefer, and W. S. Chamberlin, A two-component description of spectral absorption by marine particles, *Limnol. Oceanogr., 34*(8), 1500-1509, 1989.

Mueller, J. L., MER 2040 SN 8728: Irradiance immersion factors, *CHORS Tech. Memo. 004-96*, 3 pp., Center for Hydro-Optics and Remote Sensing, San Diego State University, San Diego CA, 1996.

Mueller, J. L., and R. W. Austin, Ocean protocols, edited by S. B. Hooker and E. R. Firestone, *NASA Tech Memo. 104566*, vol. 5, 45 pp., 1992.

Mueller, J. L., J. McLean, and B. C. Johnson, The first SeaWiFS intercalibration round-robin experiment, SIRREX-1, July 1992, edited by S. B. Hooker and E. R. Firestone, *NASA Tech Memo. 104566*, vol. 14, 58 pp., 1993.

Mueller, J. L., J. McLean, B. C. Johnson, C. L. Cromer, J. W. Cooper, J. T. McLean, S. B. Hooker, and T. L. Westphal, The second SeaWiFS intercalibration round-robin experiment, SIRREX-2, July 1993, edited by S. B. Hooker and E. R. Firestone, *NASA Tech Memo. 104566*, vol. 16, 120 pp., 1994.

Nelson, N. B., D. A. Siegel, and A. F. Michaels, Seasonal dynamics of colored dissolved material in the Sargasso Sea, *Deep-Sea Res., Part I*, in press, 1997.

Prieur, L., and S. Sathyendranath, An optical classification of coastal and oceanic waters based on the specific spectral absorption curves of phytoplankton pigments, dissolved organic matter, and other materials, *Limnol. Oceanogr., 26*(4), 671-689, 1981.

Roesler, C. S., and M. J. Perry, In situ phytoplankton absorption, fluorescence emission, and particulate backscattering spectra determined from reflectance, *J. Geophys. Res., 100*(C7), 13,279-13,294, 1995.

Roesler, C. S., M. J. Perry, and K. L. Carder, Modeling in situ phytoplankton absorption from total absorption spectra in productive inland marine waters, *Limnol. Oceanogr., 34*(8), 1510-1523, 1989.

Sathyendranath, S., L. Prieur, A. Morel, A three-component model of ocean colour and its application to remote sensing of phytoplankton pigments in coastal waters, *Int. J. Remote Sens., 10*(8), 1373-1394, 1989.

Siegel, D. A., and A. F. Michaels, Quantification of non-algal light attenuation in the Sargasso Sea: Implications for biogeochemistry and remote sensing, *Deep Sea Res., Part II, 43*, 312-345, 1996.

Siegel, D. A., R. Iturriaga, R. R. Bidigare, H. Pak, R. C. Smith, T. D. Dickey, J. Marra and K. S. Baker, Meridional variations of the springtime phytoplankton community in the Sargasso Sea, *J. Mar. Res., 48*, 379-412, 1990.

Siegel, D. A., A. F. Michaels, J. C. Sorenson, M. C. O'Brien, and M. A. Hammer, Seasonal variability of light availability and its utilization in the Sargasso Sea, *J. Geophys. Res., 100*(C5), 8695-8713, 1995a.

Siegel, D A., M. C. O'Brien, J. C. Sorenson, D. Konoff, and E. Fields, *BBOP Data Processing and Sampling Procedures, Version 1*, 79 pp., U. S. Joint Global Ocean Flux Study Plann. and Coord. Off., Woods Hole, Mass., 1995b.

Smith, R. C., and K. S Baker, Optical properties of the clearest natural waters, *Appl. Opt., 20*, 177-184, 1981.

Smith, R. C., C. R. Booth, and J. L. Star, Oceanographic biooptical profiling system, *Appl. Opt., 23*, 2791-2797, 1984.

Smith, R. C., O. B. Brown, F. E. Hoge, K. S. Baker, R. H. Evans, R. N. Swift, and W. E Esaias, Multiplatform sampling (ship, aircraft, and satellite of a Gulf Stream warm core ring), *Appl. Opt., 26*, 2068-2081, 1987.

Stramski, D., and D. A. Kiefer, Optical properties of marine bacteria, in *Ocean Optics 10, Proc. SPIE Int. Soc. Opt. Eng., 1302*, 250-268, 1990.

Stramski, D., and D. A. Kiefer, Light scattering by microorganisms in the open ocean, *Prog. Oceanogr., 28*(4), 343-383, 1991.

Sugihara, S., M. Kishino, and N. Okami, Estimation of water quality parameters from irradiance reflectance using optical models, *J. Ocean. Soc. Japan, 41*, 399-406, 1985.

Weir, C. T., D. A. Siegel, A. F. Michaels, M. C O'Brien, and D. Menzies, In situ evaluation of a ship's shadow, in *Ocean Optics 12, Proc. SPIE Int. Soc. Opt. Eng., 2258*, 815-821, 1994.

S. A. Garver and D. A. Siegel, Institute for Computational Earth System Science and Department of Geography, University of California, Santa Barbara, CA 93106.

(Received January 2, 1996; revised October 8, 1996;
accepted October 16, 1996)